bioRχiv

A Latent Clinical-anatomical Dimension Relating Metabolic Syndrome to Brain Morphology

Evidence from a Multivariate Imaging Analysis of 40,087 Individuals

Marvin Petersen[1*], Felix Hoffstaedter[2,3], Felix L. Nägele[1], Carola Mayer[1], Maximilian Schell[1], D. Leander Rimmele[1], Birgit-Christiane Zyriax[4], Tanja Zeller[5], Simone Kühn[6], Jürgen Gallinat[6], Jens Fiehler[7], Raphael Twerenbold[5,8,9,10], Amir Omidvarnia[2,3], Kaustubh R. Patil[2,3], Simon B. Eickhoff[2,3], Götz Thomalla[1], Bastian Cheng[1]

[1] Department of Neurology, University Medical Center Hamburg-Eppendorf, Hamburg, Germany
[2] Institute for Systems Neuroscience, Medical Faculty, Heinrich-Heine University Düsseldorf, Düsseldorf, Germany
[3] Institute of Neuroscience and Medicine, Brain and Behaviour (INM-7), Research Center Jülich, Jülich, Germany
[4] Midwifery Science-Health Services Research and Prevention, Institute for Health Services Research in Dermatology and Nursing (IVDP), University Medical Center Hamburg-Eppendorf, 20246 Hamburg, Germany
[5] Department of Cardiology, University Heart and Vascular Center, Hamburg, Germany
[6] Department of Psychiatry and Psychotherapy, University Medical Center Hamburg-Eppendorf, Hamburg, Germany
[7] Department of Diagnostic and Interventional Neuroradiology, University Medical Center Hamburg-Eppendorf, Hamburg, Germany
[8] Epidemiological Study Center, University Medical Center Hamburg-Eppendorf, Hamburg, Germany
[9] German Center for Cardiovascular Research (DZHK), partner site Hamburg/Kiel/Luebeck, Hamburg, Germany
[10] University Center of Cardiovascular Science, University Heart and Vascular Center, Hamburg, Germany

*Correspondence should be addressed to M.P. (mar.petersen@uke.de)

Metabolic syndrome (MetS) describes the clustered prevalence of abdominal obesity, arterial hypertension, dyslipidemia and insulin resistance, collectively promoting cerebrovascular disease. Although this risk factor complex causes a substantial health burden in modern societies, its neural underpinnings remain elusive. To investigate the multivariate association of MetS and cortical thickness, we applied partial least squares (PLS) correlation to a pooled sample of two large-scale population-based cohort studies totaling 40,087 individuals. PLS identified a latent clinical-anatomical dimension relating more severe MetS with a widespread pattern of cortical thickness abnormalities and worse cognitive performance. MetS effects were strongest in regions with high density of endothelial cells, microglia and excitatory neurons of subtype 8. Moreover, regional MetS effects correlated within functionally and structurally connected networks. Overall, our research suggests a low-dimensional relationship between MetS and brain structure that is governed by both the microscopic composition of brain tissue as well as macroscopic brain network organization.

Introduction

Metabolic syndrome (MetS) refers to the clustered appearance of multiple vascular risk factors.[1] With its high prevalence of 23-35% in Western societies, MetS constitutes a significant health burden promoting cardio- and cerebrovascular diseases.[2–4] According to the consensus definition of the *International Diabetes Federation*, MetS components comprise abdominal obesity, arterial hypertension, dyslipidemia and insulin resistance.[5] The causes of MetS are complex, with a high-fat diet, a sedentary lifestyle, and genetic predisposition ranking among the most important risk factors.[1] Importantly, lifestyle changes and pharmaceutical intervention can modify the disease course of MetS.[1] Neurological sequelae include increased risk of stroke, cognitive decline and dementia, which form a substantial public health challenge.[6–9] Therefore, advancing our understanding of the pathophysiological effects of MetS on brain structure and function as potential mediators of MetS-related neurological diseases is of high relevance.

Magnetic resonance imaging (MRI) enables in-vivo assessment of disease effects on brain structure. Few studies report associations between MetS and structural brain changes. Among them, altered cortical grey matter morphology in the form of lower cortical thickness represents the most consistent finding.[10] Yet, the current understanding of the relationship between MetS and brain structure is limited for several reasons. To date, there have been only few studies on MetS effects on cortical grey matter integrity that are well-powered.[11–13] The majority of analyses are based on small sample sizes and report effects only on global measures of brain morphology or a priori-defined regions of interest, limiting their scope.[13–18] As a result, reported effects are heterogeneous and most likely difficult to reproduce.[19] In addition, existing large-scale analyses on the isolated effects of individual risk factors (such as hypertension or obesity) do not account for the high covariance of MetS components driven by interacting pathophysiological effects, which may prevent them from capturing the whole picture of MetS effects on the brain.[16,20–25] For instance, endothelial dysfunction as a pathophysiological

substrate of structural brain injury might not only be caused by shearing effects due to arterial hypertension but also by obesity-associated chronic inflammation.[24] Furthermore, of the few well-powered studies on MetS, all are based on a case-control design.[11–13] Such group comparisons provide a statistically straightforward way to analyze MetS effects. However, they are ill-suited to assess MetS as a risk factor composite as they do not account for a dose-dependent, continuous nature of risk-related effects. Moreover, group comparisons ignore that individual MetS components might differentially contribute to abnormal brain anatomy. Lastly, analyses addressing the complex interrelationship of MetS, brain structure and cognitive functioning by investigating them in conjunction are scarce.[10,14]

Although the effects of MetS on brain structure were reported previously, its spatial distribution, potentially relating to differential vulnerability of brain regions, remains opaque. A growing body of evidence shows that brain pathology in general is shaped by multi-scale neurobiological processes, ranging from the cellular level to regional dynamics to large-scale brain networks.[26,27] On the one hand, disease effects can be driven by local properties, when local patterns of tissue composition predispose individual regions to pathology.[28–30] On the other hand, disease effects on the cerebral cortex are linked to topological properties of structural and functional brain networks. For instance, neurodegenerative and neurodevelopmental diseases appear to preferentially target brain areas with distinguished network embedding – e.g., network nodes with high connectivity and prominent topological location.[31,32] Cortical atrophy also coincides within highly connected brain areas, so-called network neighborhoods.[33,34]

Taken together, there is a need for further investigations in large-scale datasets of clinical and brain imaging data designed to take into account multiple aspects: (1) the investigation of MetS effects on the integrity of the cerebral cortex and its spatial distribution; (2) the assessment of determinants of this effect pattern; (3) a balance of resolving individual contributions of MetS components to brain structure while accounting for their high covariance and (4) the consideration of impaired cognitive function as a relevant sequel of MetS.

To meet these research needs, we investigated cortical thickness measurements in a pooled sample of two large-scale population-based cohorts from the UK Biobank (UKB) and Hamburg City Health Study (HCHS) comprising in total 40,087 participants. Partial least squares correlation analysis (PLS) was employed to characterize MetS effects on regional cortical morphology.[5,35] PLS is especially suitable for this research task as it identifies overarching latent relationships by establishing a data-driven multivariate mapping between MetS components and cortical thickness. Furthermore, capitalizing on the cognitive phenotyping of both investigated cohorts, we examined the interrelation between MetS, cognitive function and cortical thickness. Lastly, to uncover the determinants underlying differential MetS effects on cortical areas, we mapped local cellular as well as network topological attributes to observed MetS-associated cortical abnormalities. With this work, we aimed to advance the understanding of the fundamental principles underlying the neurobiology of MetS.

Results

Sample characteristics

Application of exclusion criteria and quality assessment ruled out 2,188 UKB subjects and 30 HCHS subjects resulting in a final analysis sample of 40,087 individuals. For a flowchart providing details on the sample selection procedure please refer to *supplementary figure S1*. Descriptive statistics are listed in *Table 1*. To sensitivity analyze our results, as well as to facilitate the comparison with previous reports which primarily rely on a case-control design, we supplemented group statistics comparing individuals with clinically defined MetS and matched controls, where applicable. Corresponding group analysis results are described in more detail in *supplementary materials S2-8.*

Partial least squares correlation

We investigated the relationship between cortical thickness and clinical measures of MetS (abdominal obesity, arterial hypertension, dyslipidemia, insulin resistance) in a partial least squares correlation analysis (PLS) considering all individuals from both studies (N=40,087). By this, we aimed to detect the continuous effect of any MetS component independent from a formal binary classification of MetS (present / not present). A correlation matrix relating all considered MetS component measures is displayed in supplementary figure S9. Before conducting the PLS, cortical thickness and clinical data were deconfounded for age, sex, education and cohort effects.

PLS identified seven significant latent variables relating MetS components to cortical thickness (supplementary table S10). The first latent variable explained 77.48% of shared variance and was thus further investigated (figure 1a). Specifically, the first latent variable corresponded with a covariance pattern of lower severity of MetS (figure 1b; loadings [95% confidence interval]; waist circumference: -.228 [-.237,-.219], hip circumference: -.188 [-.197,-.179], waist-hip ratio: -.162 [-.171,-.152], body mass index: -.230 [-.239,-.221], systolic blood pressure: -.098 [-.108,-.089], diastolic blood pressure: -.121 [-.131,-.112], high density lipoprotein: .096 [.087,.106], low density lipoprotein: -.013 [-.023,-.004], total cholesterol: .002 [-.008,.011], triglycerides: -.092 [-.101,-.082], glucose: -.049 [-.058,-.040]). Notably, the obesity-related measures showed the strongest contribution to the covariance profile as indicated by the highest loading to the latent variable. Age (.004 [-.006,.013]), sex (.004 [-.005,.014]), education (.002 [-.007,.010]) and cohort (.001 [-.008,.010]) did not significantly contribute to the latent variable, which is compatible with sufficient effects of deconfounding. Details on the

second latent variable which explained 17.26% of shared variance are provided in supplementary figure S11.

Bootstrap ratios were computed to identify cortical regions with a significant contribution to the covariance profile (see Methods). Cortical thickness in orbitofrontal, lateral prefrontal, insular, anterior cingulate and temporal areas contributed positively to the covariance pattern as indicated by a positive bootstrap ratio (figure 1c). Thus, a higher cortical thickness in these areas corresponded with less obesity, hypertension, dyslipidemia and insulin resistance and vice versa, i.e., lower cortical thickness with increased severity of MetS. A negative bootstrap ratio was found in superior frontal, parietal and occipital regions indicating that a higher cortical thickness in these regions corresponded with a more pronounced expression of MetS components. This overall pattern was confirmed via conventional, vertex-wise group comparisons of cortical thickness measurements based on the binary classification of individuals with MetS and matched controls (supplementary figure S8) as well as subsample analyses considering the UKB and HCHS participants independently (supplementary figure S12-13). The correlation matrix of all spatial effect maps investigated in this study (bootstrap ratio and Schaefer400-parcellated t-statistic from group comparisons) is visualized in supplementary figure S14. All derived effect size maps were significantly correlated (r_{sp}=.70 - .99, p_{FDR} < .05).

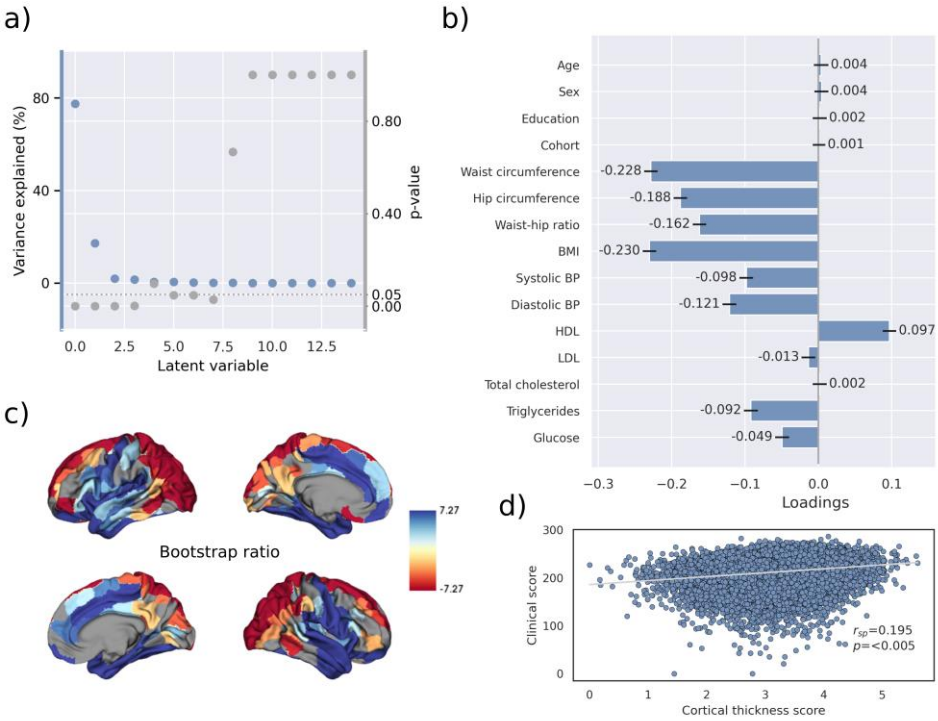

Figure 1. *Partial least squares (PLS) analysis from all individuals included in the analysis (n = 40,087). a) Explained variance and p-values of latent variables. b) Clinical covariance profile. 95% confidence intervals were calculated via bootstrap resampling. Note that confound removal for age, sex, education and cohort was performed prior to PLS. c) Bootstrap ratio representing the covarying cortical thickness pattern. A high positive or negative bootstrap ratio indicates high contribution of a brain region to the overall covariance pattern. Vertices with a significant bootstrap ratio (> 1.96 or < -1.96) are highlighted by colors. d) Scatter plot relating subject-specific clinical and cortical thickness scores. Higher scores indicate higher adherence to the respective covariance profile. Abbreviations: r_{sp} - Spearman correlation coefficient.*

Subject-specific cortical thickness and clinical scores for the first latent variable were computed. These scores indicate to which degree an individual expresses the corresponding covariance profiles. By definition, the scores are correlated (r_{sp} = .195, p<.005, figure 1d) indicating that individuals exhibiting the clinical covariance pattern (severity of MetS components) also express the cortical thickness pattern. This relationship was robust across a 10-fold cross-validation (avg. r_{sp} = .21, supplementary table S15).

To examine the interrelationship of cortical thickness, MetS components and cognition, we conducted the PLS in the UKB sample and the HCHS sample, separately, as the cognitive assessment varied between UKB and HCHS. Within the individual cohorts, cognitive variables were included in the PLS as clinical variables alongside MetS components. The resulting first latent variable associated a more severe risk profile with lower cortical thickness, but also worse cognitive performance as shown by respective loadings. Significant cognitive loadings in the UKB analysis were identified for the Fluid Intelligence Test (loadings [95% confidence interval]; .063 [.053,.072]), Matrix Pattern Completion Test (.054 [.044,.064]), Numeric Memory Test (.032 [.022,.041]), Paired Associate Learning Test (.051 [.041,.060]), Reaction Time Test (-.040 [-.049,-.030]), Symbol Digit Substitution Test (.040 [.030,.050]), Tower Rearranging Test (.035 [.025,.045]) and Trail Making Test Part B (-.019 [-.029,-.009]) (supplementary figure S12b). A significant HCHS-specific cognitive loading was found for the Multiple-choice Vocabulary Intelligence Test (.070 [.031,.109]) (supplementary figure S13b). Supplementary group comparisons of cognitive measures within the UKB and HCHS subsamples are provided in supplementary tables S5-6.

Contextualization of cortical thickness alterations

We investigated whether the pattern of MetS effects on cortical structure is conditioned by the regional density of specific cell populations and global brain network topology in a surface-based contextualization analysis.

Therefore, we first used a virtual histology approach to relate the bootstrap ratio from PLS to the differential expression of cell-type specific genes based on microarray data

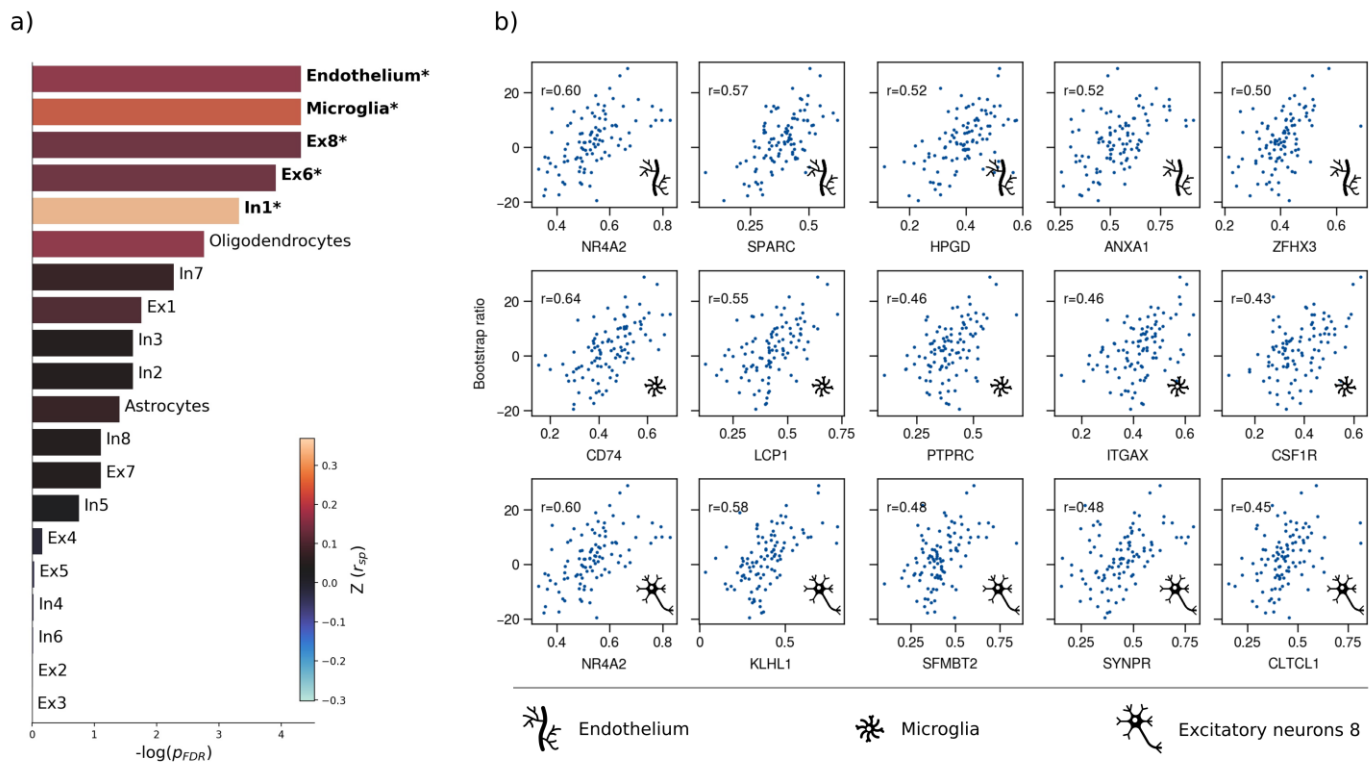

Figure 2. Virtual histology analysis. The correspondence between MetS effects (bootstrap ratio) and cell type-specific gene expression profiles was examined via an ensemble-based gene category enrichment analysis. a) Barplot displaying spatial correlation results. The bar height displays the significance level. Colors encode the aggregate z-transformed Spearman correlation coefficient relating the Schaefer100-parcellated bootstrap ratio and respective cell population densities. b) Scatter plots illustrating spatial correlations between MetS effects and exemplary cortical gene expression profiles per cell population significantly associated across analyses – i.e., endothelium, microglia and excitatory neurons type 8. Top 5 genes most strongly correlating with the bootstrap ratio map were visualized for each of these cell populations. Icons in the bottom right of each scatter plot indicate the corresponding cell type. A legend explaining the icons is provided at the bottom. First row: endothelium; second row: microglia; third row: excitatory neurons type 8. A corresponding plot illustrating the contextualization of the t-statistic derived from group statistics is shown in supplementary figure S17. Abbreviations: $-log(p_{FDR})$ – negative logarithm of the false discovery rate-corrected p-value derived from spatial lag models112,114; r – Spearman correlation coefficient. $Z(r_{sp})$ – aggregate z-transformed Spearman correlation coefficient.

from the Allen Human Brain Atlas. The results are illustrated in figure 2. The bootstrap ratio was significantly positively correlated with the density of endothelial cells ($Z_{r_{sp}}$ = .192, p_{FDR} = .013), microglia ($Z_{r_{sp}}$ = .268, p_{FDR} = .013), excitatory neurons type 8 ($Z_{r_{sp}}$ = .166, p_{FDR} = .013), excitatory neurons type 6 ($Z_{r_{sp}}$ = .156, p_{FDR} = .002) and inhibitory neurons type 1 ($Z_{r_{sp}}$ = .368, p_{FDR} = .036) indicating that MetS effects on cortical thickness are strongest in regions of the highest density of these cell types. No significant associations were found with regard to the remaining excitatory neuron types (Ex1-Ex5, Ex7), inhibitory neurons (In2-In8), astrocytes and oligodendrocytes (supplementary table S16). As a sensitivity analysis, we contextualized the t-statistic map derived from group statistics. The results remained stable except for excitatory neurons type 6 ($Z_{r_{sp}}$ = .145, p_{FDR} = .123) and inhibitory neurons type 1 ($Z_{r_{sp}}$ = .432, p_{FDR} = .108), which no longer showed a significant association (supplementary materials S17-18).

Second, we associated the bootstrap ratio with three preselected measures of brain network topology derived from group consensus functional and structural connectomes (figure 3): weighted degree centrality (marking brain network hubs), neighborhood abnormality and macroscale functional connectivity gradients.[36] The bootstrap ratio showed a medium positive correlation with the functional neighborhood abnormality (r_{sp} = .452, p_{spin} = .002, p_{smash} < .001, p_{rewire} < .001) and a strong positive correlation with the structural neighborhood abnormality (r_{sp} = .770, p_{spin} = <.001, p_{smash} < .001, p_{rewire} < .001) indicating functional and structural interconnectedness of areas experiencing similar MetS effects. These results remained significant when the t-statistic map was contextualized instead of the bootstrap ratio as well as when neighborhood abnormality measures were derived from consensus connectomes of the HCHS instead of the Human Connectome Project (supplementary figure S19-20). We found no significant associations for the remaining indices of network topology, i.e., functional degree centrality (r_{sp} = .162, p_{spin} = .362, p_{smash} = .362, p_{rewire} = .876), structural degree centrality (r_{sp} = .038, p_{spin} = .393, p_{smash} = .828, p_{rewire} = .082) as well as functional cortical gradient 1 (r_{sp} = .159, p_{spin} = .293, p_{smash} = .362, p_{rewire} = .018) and gradient 2 (r_{sp} = -.190, p_{spin} = .293, p_{smash} = .362, p_{rewire} = .001).

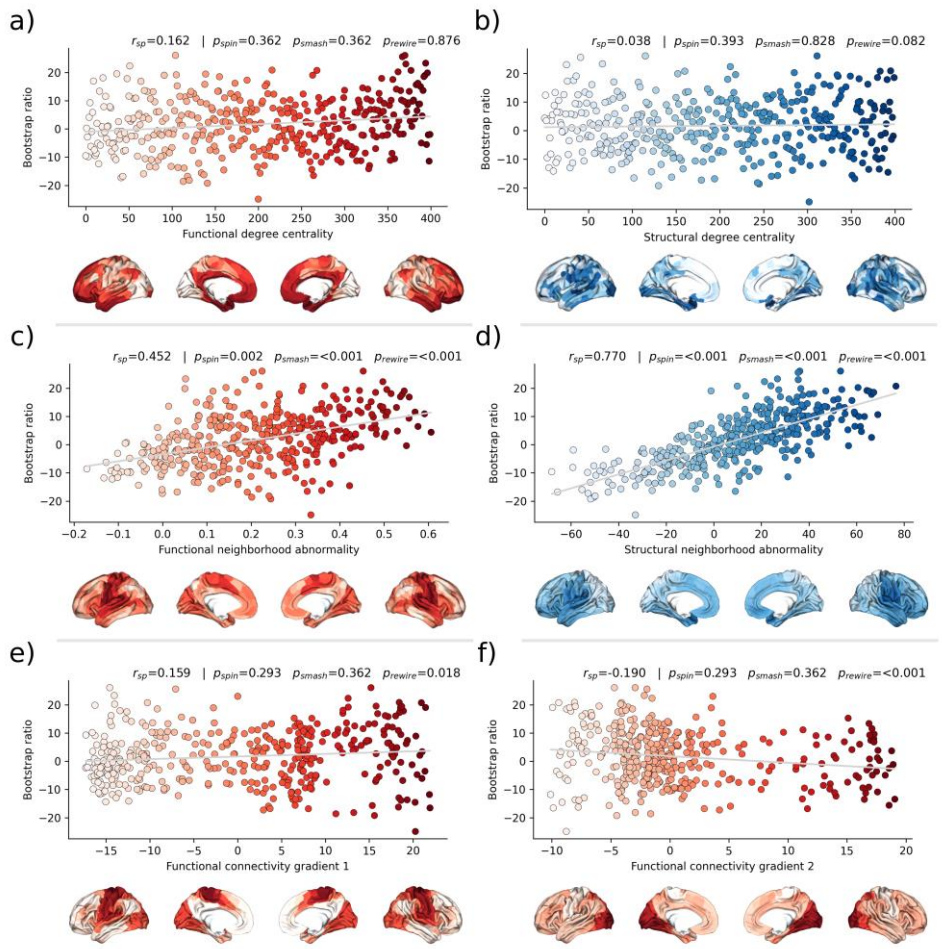

Figure 3. Brain network contextualization. Spatial correlation results derived from relating Schaefer400x7-parcellated cortical maps of MetS effects (bootstrap ratio) to network topological indices (red: functional connectivity, blue: structural connectivity). Scatter plots that illustrate the spatial relationship are supplemented by respective surface plots for anatomical localization. The color coding of cortical regions and associated dots corresponds. a) & b) Functional and structural degree centrality rank. c) & d) Functional and structural neighborhood abnormality. e) & f) Intrinsic functional network hierarchy represented by functional connectivity gradients 1 and 2. Complementary results concerning t-statistic maps derived from group comparisons between MetS subjects and controls are presented in supplementary figure S19. Abbreviations: p_{rewire} - p-value derived from network rewiring[121]; p_{smash} - p-value derived from brainSMASH surrogates[95]; p_{spin} - p-value derived from spin permutation results[120]; r_{sp} - Spearman correlation coefficient.

Discussion

We investigated the impact of metabolic syndrome on cortical thickness and cognitive functions in a large sample of individuals from two epidemiological neuroimaging studies. We report three main findings: (1) The relationship between MetS and cortical thickness showed a low-dimensional structure: one single latent variable relating lower cortical thickness to more severe MetS explained most of the variance; (2) MetS was associated with lower cortical thickness in orbitofrontal, lateral prefrontal, insular, cingulate and temporal cortices. Lower cortical thickness in these areas covaried with overall worse performance in cognitive tests; (3) The pattern of MetS-effects on cortical thickness appeared to be conditioned by regional cell composition as well as functional and structural connectivity. These findings were robust across sensitivity analyses. Collectively, our study provides a comprehensive assessment of the multifaceted relationship between MetS and brain structure.

MetS affects brain health in a complex manner with interacting effects on the cerebral vasculature and parenchyma as shown by histopathological and imaging studies.[24] Pathophysiological aspects of MetS comprise (1) atherosclerosis impairing parenchymal blood supply by promoting acute and chronic hypoperfusion as well as triggering inflammatory processes;[37–39] (2) endothelial dysfunction leading to diminished cerebral vasoreactivity rendering the vasculature less responsive to stimuli tailoring the blood flow to the brains metabolic needs;[40,41] (3) blood-brain barrier breakdown causing plasma proteins and immunoglobulins to enter neural tissue while the efflux of waste products is hindered collectively inducing an inflammatory response;[42] (4) oxidative stress impairing neuronal integrity and leading to mitochondrial dysfunction.[43] Together, these effects culminate in (5) small vessel injury causing a variety of pathologies – inter alia, white matter damage, microinfarcts and cerebral microbleeds.[44,45]

To address these interacting effects, we harnessed multivariate statistics in form of a partial least squares correlation analysis (PLS) in two large-scale population-based studies to probe for covariance profiles relating the full range of MetS components (such as obesity or arterial hypertension) to cortical thickness in a single analysis. PLS successfully identified seven significant latent variables with the first variable explaining the majority (77.48%) of shared variance within the imaging and clinical data (figure 1a). This finding suggests that the overall relationship of MetS and brain structure is low-dimensional, i.e., effects of MetS components on cortical thickness are relatively uniform despite the diversity of underlying pathomechanisms. PLS revealed that all MetS components were contributing to this latent signature, suggesting overlapping effects. Waist circumference, hip circumference, waist-hip ratio and body mass index consistently contributed higher than the remaining variables across conducted analyses which highlights obesity as the strongest driver of MetS-related cortical morphometric abnormalities.

We interpret these findings as evidence that MetS-associated conditions jointly contribute to the harmful effects on brain structure rather than affecting it in a strictly individual manner. This notion is supported by previous work in the UKB demonstrating overlapping effects of individual vascular risk factors on cortical morphology.[23] Specifically, the covariance profile corresponding with the first latent variable signified that increased severity of obesity, dyslipidemia, arterial hypertension and insulin resistance was associated with lower cortical thickness in orbitofrontal, lateral prefrontal, insular, cingulate and temporal cortices (figure 1b and 1c). This profile was coherently observed across complementary analyses including "conventional" group comparisons based on binary classifications of MetS as well as separate analyses of UKB and HCHS data (supplementary figure S14). Our findings are in line with previous evidence highlighting a frontotemporal morphometric abnormality pattern associated with MetS.[14,46,47] As a speculative causative pathway, human and animal studies have related the orbitofrontal, insular and anterior cingulate cortex to food-related reward processing, taste and impulse regulation.[48–52] Conceivably, structural alterations of these brain regions are linked to brain functions and behaviors that exacerbate the risk profile leading to MetS.[53,54] However, further work is needed to test this hypothesis. Interestingly, we also observed a positive relationship between cortical thickness and MetS in the superior frontal, parietal and occipital lobe. Interpretation of this result is, however, less intuitive. Analyses on dyslipidemia have reported positive correlations with cortical thickness before.[47,55] As neurodegenerative processes have been associated with a disruption of brain cholesterol production, increased levels of serum cholesterol levels in MetS might compensate this relative deficiency.[56,57]

Cognitive performance has been consistently linked to vascular risk factors and structural brain abnormalities in health and disease.[58] We investigated the interrelationship between MetS, cortical thickness and cognitive function in a complementary analysis. Applying PLS to both datasets (UKB and HCHS) individually revealed that the identified latent variables were characterized by more severe MetS, lower cortical thickness and worse cognitive performance (supplementary materials S12b and S13b). These associations were replicated by results from the group comparison highlighting worse performance in several cognitive domains in MetS (supplementary tables S5-6) being in line with previous reports.[10,59–61] As a potential mechanism underlying these associations, altered cortical structure has been shown to mediate the relationship between MetS and cognitive performance in a pediatric study and elderly patients with vascular cognitive impairment.[62–64] The detected latent variable might represent a continuous disease spectrum spanning from minor cognitive deficits due to MetS-associated vascular risk factors to more severe vascular cognitive impairment and dementia. In support of this hypothesis, the determined cortical thickness covariance pattern is consistent with the atrophy pattern found in vascular mild cognitive impairment and vascular dementia.[63,64] Collectively, we interpret these findings as evidence for an interrelationship between MetS, cognitive dysfunction and structural brain alteration.

To better understand the emergence of the spatially distinctive anatomical pattern of MetS effects on cortical thickness, we conducted two brain surface-based contextualization analyses based on reference datasets of (1) local gene expression data and (2) properties of brain network topology.

For the first approach, we performed a virtual histology analysis harnessing regional gene expression data. Specifically, we assessed whether differential MetS effects correspond with the density of certain cell populations as determined by transcriptional activity using microarray measurements from the Allen Human Brain Atlas (figure 2). As the main finding, we report an association between the MetS-related anatomical pattern of lower cortical thickness and higher regional density of endothelial cells – i.e., the cells constituting the lining of blood vessels. As endothelial dysfunction is a core pathomechanistic correlate of MetS,[40,41] this association is generally plausible. Endothelial dysfunction compromises neural tissue via chronic vascular inflammation, increased thrombosis risk and hypoperfusion due to altered vasoreactivity and vascular remodelling, leading to loss of structural neuronal integrity and cortical atrophy.[65] We interpret our findings as an indication for increased susceptibility of brain regions with high endothelial density to MetS-related effects of cortical disintegration. As endothelial density serves as a proxy for the degree of general tissue vascularization, well-vascularized regions are also likely to be more vulnerable to MetS and its related cluster of vascular risk factors.[37] Our results furthermore indicate that microglial density determines a brain region's susceptibility to MetS effects. Microglia are resident macrophages of the central nervous system sustaining neuronal integrity by maintaining a healthy microenvironment. Animal studies have linked chronic neuroinflammation mediated by blood-brain barrier leakage and systemic inflammation to vascular risk.[66,67] Activated microglia can also harm the brain structure by releasing reactive oxygen species, proinflammatory cytokines and proteinases.[68] Lastly, we found an association with the density of excitatory neurons of subtype 8. These neurons reside in cortical layer 6 and their axons mainly entertain cortico-thalamic and callosal connections.[69] The trajectories of these long fascicles run through the deep and periventricular white matter, i.e., distant from well-perfused pericortical areas rendering them reliant on branches of small perforating brain vessels, commonly affected in CSVD.[70–72] Consequently, layer 6 neurons might be preferentially susceptible to MetS effects due to their exposition to vascular risk-related white matter disease. Taken together, the virtual histology analysis indicates that MetS effects on cortical thickness are conditioned by local cellular fingerprints. Our results underscore the role of endothelial cells and microglia in MetS-related vascular risk factors affecting the structural integrity of the cerebral cortex.

For the second approach, we contextualized MetS-effects on cortical thickness using principal topological properties of functional and structural brain networks. We found that regional MetS effects and those of functionally and structurally connected neighbors were correlated (figure 3d) - i.e., areas with similar MetS effects tended to be disproportionately interconnected. Put differently, MetS effects coincided within functional and structural brain networks. Therefore, our findings provide evidence that a region's functional and structural network embedding – i.e., its individual fingerprint of functional interactions as well as white matter fiber tract connections - determines its susceptibility to morphometric MetS effects. Multiple mechanisms might explain how connectivity conditions the cortical alterations related to MetS. For example, microvascular pathology might impair white matter fiber tracts leading to joint degeneration in interconnected cortical brain areas:[73,74] that is, the occurrence of shared MetS effects within functionally and structurally connected neighborhoods is explained by their shared (dis-)connectivity profile. In support of this, previous work using diffusion tensor imaging suggests that MetS-related microstructural white matter alterations prefentially occur in the frontal and temporal lobe, which spatially matches the frontotemporal morphometric differences observed in our work.[75] Furthermore, we speculate on an interplay between local and network-topological susceptibility in MetS: functional and structural connectivity may provide a scaffold for propagating MetS-related perturbation across the network in the sense of a spreading phenomenon - i.e., a region might be influenced by network-driven exposure to regions with higher local susceptibility. Observed degeneration of a region might be aggravated by malfunctional communication to other vulnerable regions including mechanisms of excitotoxicity, diminished excitation and metabolic stress.[76]

This work has strengths and limitations. The strengths of this work include the very large sample size with marked statistical power for exploring associations between imaging, demographic and behavioral data;[19] high-quality multimodal MRI and clinical data; state-of-the art, large-scale, robust and reproducible image processing; and a comprehensive methodology including a modern multivariate statistical approach to explore the nature of MetS effects on brain structure supplemented by multimodal contextualization analyses to advance the pathophysiological understanding of this relationship. Several limitations should be mentioned. The virtual histology analysis relied on gene expression information from the Allen Human Brain Atlas which is based on samples of post-mortem brains. In-vivo sampling might have resulted in different gene expression profiles, which should be considered if interpreting our results. In addition, the number of UKB subjects in our study markedly exceeds that of HCHS subjects. Therefore, the results may be influenced by this overrepresentation. A further limitation of this work lies in its cross-sectional design, which restricts the ability for demonstrating causative effects. Although considerable human and technical resources are necessary to conduct a longitudinal study of similar size and scope, longitudinal assessment of the surveyed relationships would provide more robust evidence and therefore, future studies should move in this direction.

Conclusion

We performed a comprehensive assessment of the association between MetS and brain structure to contribute to deciphering the complex relationship of vascular risk and brain health. Integrated data-driven statistics revealed a single clinical-anatomical dimension explaining most variance of this association, highlighting its low-dimensional nature. Concomitantly, a characteristic and reproducible structural imaging fingerprint associated with MetS was identified. This pattern of MetS-related brain morphological abnormalities was governed by local histological as well as global network topological features. Collectively, our results highlight how an integrative, multi-modal analysis approach can lead to a more holistic understanding of the neural underpinnings of MetS and its vascular risk components. The clinical-anatomical dimension identified here opens a new opportunity for dimensional stratification of vascular risk, complementing existing efforts to motivate and inform prevention strategies.

Materials and methods

Study population

Here, we investigated cross-sectional clinical and imaging data from two large-scale population-based cohort studies: (1) the UK Biobank (UKB, n = 39,668, age 45-80 years; application numbers 71359 and 41655) and (2) the Hamburg City Health Study (HCHS, n = 2637, age 45-74 years).[77,78] Both studies recruit large study samples with neuroimaging data alongside detailed demographic and clinical assessment. Respectively, data for the first visit including a neuroimaging assessment were included. Individuals were excluded if they had a history or a current diagnosis of neurological or psychiatric disease. UKB individuals were excluded based on the non-cancer illnesses codes (http://biobank.ndph.ox.ac.uk/showcase/coding.cgi?id=6). Excluded conditions were Alzheimer's disease; alcohol, opioid and other dependencies; amyotrophic lateral sclerosis; brain injury; brain abscess; chronic neurological problem; encephalitis; epilepsy; haemorrhage; head injury; meningitis; multiple sclerosis; Parkinson's disease; skull fracture.[79] Same criteria were applied on HCHS individuals based on the neuroradiological evaluation and self-reported diagnoses variables. To enhance comparability to previous studies we supplemented a case-control analysis enabling to complement continuous multivariate statistical analyses by group statistics. Therefore, a MetS sample was identified based on the consensus definition of the *International Diabetes Federation* (*supplementary text S21*) and matched to a control cohort. Corresponding procedures are presented in more detail in *supplementary text S2*.

Ethics approval

The UKB was ethically approved by the North West Multi-Centre Research Ethics Committee (MREC). Details on the

UKB Ethics and Governance framework are provided online (https://www.ukbiobank.ac.uk/media/0xsbmfmw/egf.pdf). The HCHS was approved by the local ethics committee of the Landesärztekammer Hamburg (State of Hamburg Chamber of Medical Practitioners, PV5131). Good Clinical Practice (GCP), Good Epidemiological Practice (GEP) and the Declaration of Helsinki were the ethical guidelines that governed the conduct of the HCHS.[72] Written informed consent was obtained from all participants investigated in this work.

Clinical assessments

In the UK Biobank, a battery of cognitive tests is administered, most of which represent shortened and computerized versions of established tests aiming for comprehensive and concise assessment of cognition.[80] From this battery we investigated tests for executive function and processing speed (Reaction Time Test, Symbol Digit Substitution Test, Tower Rearranging Test, Trail Making Tests parts A and B), memory (Numeric Memory Test, Paired Associate Learning Test, Prospective Memory Test) and reasoning (Fluid Intelligence Test, Matrix Pattern Completion Test). Detailed descriptions of the individual tests can be found elsewhere.[81] Furthermore, some tests (Matrix Pattern Completion Test, Numeric Memory Test, Paired Associate Learning Test, Symbol Digit Substitution Test, Trail Making Test and Tower Rearranging Test) are only administered to a subsample of the UKB imaging cohort explaining the missing test results for a subgroup of participants.

In the HCHS, cognitive testing was administered by a trained study nurse and included the Animal Naming Test, Mini Mental State Exam, Trail Making Test Part A and B, Verbal Fluency and Word List Recall subtests of the Consortium to Establish a Registry for Alzheimer's Disease Neuropsychological Assessment Battery (CERAD-Plus), as well as the Clock Drawing Test.[82–86]

MRI acquisition

The full UKB neuroimaging protocol can be found online (https://biobank.ctsu.ox.ac.uk/crystal/crystal/docs/brain_mri.pdf).[77] MR images were acquired on a 3-T Siemens Skyra MRI scanner (Siemens, Erlangen, Germany). T1-weighted MRI used a 3D MPRAGE sequence with 1-mm isotropic resolution with the following sequence parameters: repetition time = 2000 ms, echo time = 2.01 ms, 256 axial slices, slice thickness = 1 mm, and in-plane resolution = 1 x 1 mm. In the HCHS, MR images were acquired as well on a 3-T Siemens Skyra MRI scanner. Measurements were performed with a protocol as described in previous work.[72] In detail, for 3D T1-weighted anatomical images, rapid acquisition gradient-echo sequence (MPRAGE) was used with the following sequence parameters: repetition time = 2500 ms, echo time = 2.12 ms, 256 axial slices, slice thickness = 0.94 mm, and in-plane resolution = 0.83 × 0.83 mm.

Estimation of cortical thickness

To achieve comparability and reproducibility, the preconfigured and containerized CAT12 pipeline (CAT12.7 r1743; https://github.com/m-wierzba/cat-container) was harnessed for surface reconstruction and cortical thickness measurement building upon a projection-based thickness estimation method.[87–90] Cortical thickness measures were normalized from individual to 32k fsLR surface space (conte69) to ensure vertex correspondence across subjects.[36] Individuals with a CAT12 image quality rating lower than 75% were excluded during quality assessment. To facilitate large-scale data management while ensuring provenance tracking and reproducibility, we employed the DataLad-based FAIRly big workflow for image data processing.[91,92]

Statistical analysis

Statistical computations and plotting were performed in python 3.9.7 leveraging bctpy (v. 0.6.0), brainstat (v. 0.3.6), brainSMASH (v. 0.11.0), the ENIGMA toolbox (v. 1.1.3). matplotlib (v. 3.5.1), neuromaps (v. 0.0.1), numpy (v. 1.22.3), pandas (v. 1.4.2), pingouin (v. 0.5.1), pyls (v. 0.0.1), scikit-learn (v. 1.0.2), scipy (v. 1.7.3), seaborn (v. 0.11.2) as well as in matlab (v. 2021b) using ABAnnotate (v. 0.1.1.).[93–104]

Partial least squares correlation analysis

To relate MetS components and cortical morphology, we performed a partial least squares correlation analysis (PLS) using pyls (https://github.com/rmarkello/pyls). PLS identifies covariance profiles that relate two sets of variables in a data-driven double multivariate analysis.[35] Here, we related regional cortical thickness measures to clinical measurements of MetS components, i.e., obesity (waist circumference, hip circumference, waist-hip ratio, body mass index), arterial hypertension (systolic blood pressure, diastolic blood pressure), dyslipidemia (high density lipoprotein, low density lipoprotein, total cholesterol, triglycerides) and insuline resistance (blood glucose). Before conducting the PLS, missing values were imputed via k-nearest neighbor imputation ($n_{neighbor}$=4) with imputation only taking into account variables of the same group, i.e., MetS component variables were imputed based on the remaining MetS component data only and not based on demographic variables. To account for age, sex, education and cohort (UKB/HCHS) as potential confounds, they were regressed out of cortical thickness and MetS component data.

We then performed PLS as described in previous work.[36] Methodological details are covered in *figure 4a* and *supplementary text S22*. Cortical thickness measures were randomly permuted (n=5000) to assess statistical significance of derived latent variables and their corresponding covariance profiles. Subject-specific PLS scores were computed, where higher scores signify stronger adherence of an individual to an identified covariance profile. Bootstrap resampling (n=5000) was performed to assess the contribution of individual variables to the thickness-clinical

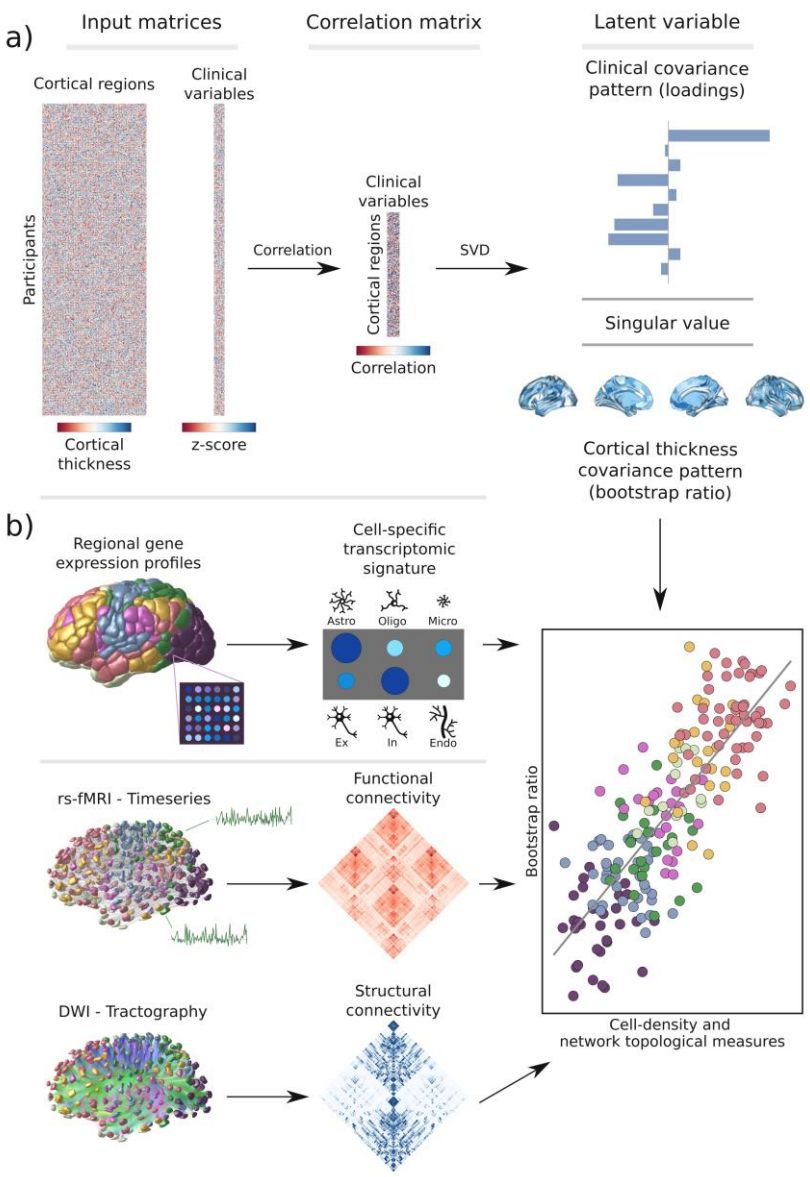

Figure 4. Methodology. a) Illustration of the partial least squares correlation analysis. Starting from two input matrices containing per-subject information of regional cortical thickness measures as well as clinical data (demographic and MetS-related risk factors) a correlation matrix is computed. This is subsequently subjected to singular value decomposition resulting in a set of mutually orthogonal latent variables. Latent variables each consist of a left singular vector (here, clinical covariance pattern), singular value and right singular vector (here, cortical thickness covariance profile). b-d) Contextualization analysis. b) Based on microarray gene expression data, the densities of different cell populations across the cortex were quantified. c) Based on functional and structural group-consensus connectomes based on data from the Human Connectome Project, metrics of functional and structural brain network topology were derived. d) Cell density as well as connectomic measures were related to the bootstrap ratio via spatial correlations. Modified from Petersen et al. and Zeighami et al.[36,122]
Abbreviations: Astro – astrocytes; DWI – diffusion-weighted magnetic resonance imaging; Endo – endothelial cells; Ex – excitatory neuron populations (Ex1-8); In – inhibitory neuron populations (In1-8); Micro – microglia; Oligo – oligodendrocytes; rs-fMRI – resting-state functional magnetic resonance imaging; SVD – singular value decomposition

relationship. Confidence intervals (95%) of singular vector weights were computed for clinical variables to assess the significance of their contribution. To estimate contributions of cortical regions, bootstrap ratios were computed as the singular vector weight divided by the bootstrap-estimated standard error. The bootstrap ratio equals a z-score in case of a normally distributed bootstrap. Hence, brain region contributions were considered significant if the bootstrap ratio was >1.96 or <-1.96 (95% confidence interval). Overall model robustness was assessed via a 10-fold cross-validation by correlating out-of-sample PLS scores within each fold.[105]

Associations of cognitive and imaging data

As cognitive assessment differed between UKB and HCHS, cognitive variables were not included in the main PLS analysis. To further explore the interrelationship of cortical thickness and cognitive measures, we reconducted the PLS on the individual cohorts including cognitive measures to the clinical variables.

Contextualization analysis

We investigated the impact of MetS on cortical thickness in the context of cell-specific gene expression profiles and structural and functional brain network characteristics. (*figure 4b-d*). Therefore, we Schaefer-parcellated (400x7 and 100x7, v.1) the bootstrap ratio map and related it to indices representing different gene expression and network topological properties of the human cortex via spatial correlations (Spearman correlation, r_{sp}) on a group-level.[106]

Virtual histology analysis. We performed a virtual histology analysis leveraging gene transcription information to quantify the density of different cell populations across the cortex. Genes corresponding with specific cell populations of the central nervous system were identified based on a classification derived from single nucleus-RNA sequencing data.[69,107] The gene-celltype mapping is provided by the PsychENCODE database (http://resource.psychencode.org/Datasets/Derived/SC_Decomp/DER-19_Single_cell_marker-genes_TPM.xlsx).[108] The abagen toolbox (v. 0.1.3) and the ENIGMA toolbox (v. 1.1.3) were used to obtain regional microarray expression data of these genes for Schaefer100x7 parcels based on the Allen Human Brain Atlas (AHBA).[109–111] The Schaefer100x7 atlas was used as it better matches the sampling density of the AHBA eventually resulting in no parcels with missing values. Regional expression patterns of genes corresponding to astrocytes, endothelial cells, excitatory neuron populations (Ex1-8),

inhibitory neuron populations (In1-8), microglia, and oligodendrocytes were extracted. Instead of assessing the correspondence between MetS effects and the expression pattern of each gene directly, we employed ensemble-based gene category enrichment analysis (GCEA) as implemented in the ABAnnotate toolbox.[104,112] This approach represents a modification to customary GCEA addressing the issues of gene-gene dependency through within-category co-expression which is caused by shared spatial embedding as well as spatial autocorrelation of cortical transcriptomics data.[113] In brief, gene transcription indices were averaged within categories (here cell populations) and spatially correlated with the bootstrap ratio map. Statistical significance was assessed by comparing the empirical correlation coefficients against a null distribution derived from surrogate maps with preserved spatial embedding and autocorrelation computed via a spatial lag model.[114]

Brain network topology. To investigate the cortical MetS effects pattern in the context of brain network topology, three connectivity metrics were leveraged based on data from structural and functional brain imaging: weighted degree centrality, neighborhood abnormality as well as macroscale functional connectivity gradients as described previously.[36] These were computed based on functional and structural consensus connectomes on group-level derived from the Human Connectome Project Young Adults dataset comprised in the ENIGMA toolbox.[96,115] Computation and derivation of the metrics are described in the *supplementary text S23*.[33,93,94,97,116–119] For this analysis, statistical significance of spatial correlations was assessed via spin permutations (n = 1,000) which represent a null model preserving the inherent spatial autocorrelation of cortical information.[120] Spin permutations are performed by projecting parcel-wise data onto a sphere which then is randomly rotated. After rotation, information is projected back on the surface and a permuted r_{sp} is computed. A p-value is computed comparing the empirical correlation coefficient to the permuted distribution. To assure that our results do not depend on null model choice, we additionally tested our results against a variogram-based null model implemented in the brainSMASH toolbox (https://github.com/murray-lab/brainsmash) as well as a network rewiring null model with preserved density and degree sequence.[95,121]

All p-values resulting from both contextualization analyses were FDR-corrected for multiple comparisons. As we conducted this study mindful of the reuse of our resources, the MetS effect maps are provided as separate supplementary files to enable further analyses.

Sensitivity analyses

To test whether the PLS indeed captures the effect of MetS on cortical thickness, we conducted a group comparison as in previous studies of MetS. Besides descriptive group statistics, individuals with MetS and matched controls were compared on a surface vertex-level leveraging the BrainStat toolbox (v 0.3.6, https://brainstat.readthedocs.io/).[94] A general linear model was applied correcting for age, sex, education and cohort effects. Vertex-wise p-values were FDR-corrected for multiple comparisons. Corresponding results can be found in *supplementary figure S8*. To demonstrate the correspondence between the t-statistic and bootstrap ratio maps, we related them via spatial correlation analyses (*supplementary figure S14*). The t-statistic map was also used to sensitivity analyze the virtual histology analysis and brain network contextualization (*supplementary materials S17-19*).

To ensure that the brain network contextualization results were not biased by the connectome choice, we reperformed the analysis with structural and functional group consensus connectomes based on resting-state functional and diffusion-weighted MRI data from the Hamburg City Health Study (*supplementary figure S20*). The corresponding connectome reconstruction approaches were described elsewhere.[36]

References

1. Eckel RH, Grundy SM, Zimmet PZ. The metabolic syndrome. *The Lancet*. 2005;365(9468):1415-1428. doi:10.1016/S0140-6736(05)66378-7

2. Aguilar M, Bhuket T, Torres S, Liu B, Wong RJ. Prevalence of the metabolic syndrome in the United States, 2003-2012. *JAMA*. 2015;313(19):1973-1974. doi:10.1001/jama.2015.4260

3. Scuteri A, Laurent S, Cucca F, et al. Metabolic syndrome across Europe: different clusters of risk factors. *Eur J Prev Cardiol*. 2015;22(4):486-491. doi:10.1177/2047487314525529

4. Beltrán-Sánchez H, Harhay MO, Harhay MM, McElligott S. Prevalence and trends of metabolic syndrome in the adult U.S. population, 1999-2010. *J Am Coll Cardiol*. 2013;62(8):697-703. doi:10.1016/j.jacc.2013.05.064

5. Alberti KGMM, Zimmet P, Shaw J. Metabolic syndrome--a new worldwide definition. A Consensus Statement from the International Diabetes Federation. *Diabet Med*. 2006;23(5):469-480. doi:10.1111/j.1464-5491.2006.01858.x

6. Boden-Albala B, Sacco RL, Lee HS, et al. Metabolic Syndrome and Ischemic Stroke Risk. *Stroke*. 2008;39(1):30-35. doi:10.1161/STROKEAHA.107.496588

7. Atti AR, Valente S, Iodice A, et al. Metabolic Syndrome, Mild Cognitive Impairment, and Dementia: A Meta-Analysis of Longitudinal Studies. *The American Journal of Geriatric Psychiatry*. 2019;27(6):625-637. doi:10.1016/j.jagp.2019.01.214

8. Razay G, Vreugdenhil A, Wilcock G. The Metabolic Syndrome and Alzheimer Disease. *Archives of Neurology*. 2007;64(1):93-96. doi:10.1001/archneur.64.1.93

9. Livingston G, Huntley J, Sommerlad A, et al. Dementia prevention, intervention, and care: 2020 report of the Lancet Commission. *The Lancet*. 2020;396(10248):413-446. doi:10.1016/S0140-6736(20)30367-6

10. Yates KF, Sweat V, Yau PL, Turchiano MM, Convit A. Impact of Metabolic Syndrome on Cognition and Brain: A Selected Review of the

Literature. *Arterioscler Thromb Vasc Biol*. 2012;32(9):2060-2067. doi:10.1161/ATVBAHA.112.252759

11. Lu R, Aziz NA, Diers K, Stöcker T, Reuter M, Breteler MMB. Insulin resistance accounts for metabolic syndrome-related alterations in brain structure. *Hum Brain Mapp*. 2021;42(8):2434-2444. doi:10.1002/hbm.25377

12. Wolf EJ, Sadeh N, Leritz EC, et al. Posttraumatic Stress Disorder as a Catalyst for the Association Between Metabolic Syndrome and Reduced Cortical Thickness. *Biological Psychiatry*. 2016;80(5):363-371. doi:10.1016/j.biopsych.2015.11.023

13. Tiehuis AM, van der Graaf Y, Mali WPTM, et al. Metabolic Syndrome, Prediabetes, and Brain Abnormalities on MRI in Patients With Manifest Arterial Disease: The SMART-MR Study. *Diabetes Care*. 2014;37(9):2515-2521. doi:10.2337/dc14-0154

14. McIntosh EC, Jacobson A, Kemmotsu N, et al. Does medial temporal lobe thickness mediate the association between risk factor burden and memory performance in middle-aged or older adults with metabolic syndrome? *Neuroscience Letters*. 2017;636:225-232. doi:10.1016/j.neulet.2016.10.010

15. Sala M, de Roos A, van den Berg A, et al. Microstructural Brain Tissue Damage in Metabolic Syndrome. *Diabetes Care*. 2014;37(2):493-500. doi:10.2337/dc13-1160

16. Tan ZS, Beiser AS, Fox CS, et al. Association of Metabolic Dysregulation With Volumetric Brain Magnetic Resonance Imaging and Cognitive Markers of Subclinical Brain Aging in Middle-Aged Adults: The Framingham Offspring Study. *Diabetes Care*. 2011;34(8):1766-1770. doi:10.2337/dc11-0308

17. Schwarz NF, Nordstrom LK, Pagen LHG, et al. Differential associations of metabolic risk factors on cortical thickness in metabolic syndrome. *Neuroimage Clin*. 2018;17:98-108. doi:10.1016/j.nicl.2017.09.022

18. Song SW, Chung JH, Rho JS, et al. Regional cortical thickness and subcortical volume changes in patients with metabolic syndrome. *Brain Imaging and Behavior*. 2015;9(3):588-596. doi:10.1007/s11682-014-9311-2

19. Marek S, Tervo-Clemmens B, Calabro FJ, et al. Reproducible brain-wide association studies require thousands of individuals. *Nature*. Published online March 16, 2022:1-7. doi:10.1038/s41586-022-04492-9

20. Hamer M, Batty GD. Association of body mass index and waist-to-hip ratio with brain structure: UK Biobank study. *Neurology*. 2019;92(6):e594-e600. doi:10.1212/WNL.0000000000006879

21. Opel N, Thalamuthu A, Milaneschi Y, et al. Brain structural abnormalities in obesity: relation to age, genetic risk, and common psychiatric disorders. *Mol Psychiatry*. 2021;26(9):4839-4852. doi:10.1038/s41380-020-0774-9

22. Schaare HL, Kharabian Masouleh S, Beyer F, et al. Association of peripheral blood pressure with gray matter volume in 19- to 40-year-old adults. *Neurology*. 2019;92(8):e758-e773. doi:10.1212/WNL.0000000000006947

23. Cox SR, Lyall DM, Ritchie SJ, et al. Associations between vascular risk factors and brain MRI indices in UK Biobank. *European Heart Journal*. 2019;40(28):2290-2300. doi:10.1093/eurheartj/ehz100

24. Borshchev YYu, Uspensky YP, Galagudza MM. Pathogenetic pathways of cognitive dysfunction and dementia in metabolic syndrome. *Life Sciences*. 2019;237:116932. doi:10.1016/j.lfs.2019.116932

25. Meigs JB, D'Agostino RB Sr, Wilson PW, Adrienne Cupples L, Nathan DM, Singer DE. Risk Variable Clustering in the Insulin Resistance Syndrome: The Framingham Offspring Study. *Diabetes*. 1997;46(10):1594-1600. doi:10.2337/diacare.46.10.1594

26. Fornito A, Zalesky A, Breakspear M. The connectomics of brain disorders. *Nature Reviews Neuroscience*. 2015;16(3):159-172. doi:10.1038/nrn3901

27. van den Heuvel MP, Sporns O. A cross-disorder connectome landscape of brain dysconnectivity. *Nature Reviews Neuroscience*. 2019;20(7):435-446. doi:10.1038/s41583-019-0177-6

28. Seidlitz J, Nadig A, Liu S, et al. Transcriptomic and cellular decoding of regional brain vulnerability to neurogenetic disorders. *Nat Commun*. 2020;11(1):3358. doi:10.1038/s41467-020-17051-5

29. Vlassenko AG, Vaishnavi SN, Couture L, et al. Spatial correlation between brain aerobic glycolysis and amyloid-β (Aβ) deposition. *Proc Natl Acad Sci U S A*. 2010;107(41):17763-17767. doi:10.1073/pnas.1010461107

30. Buckner RL, Snyder AZ, Shannon BJ, et al. Molecular, structural, and functional characterization of Alzheimer's disease: evidence for a relationship between default activity, amyloid, and memory. *J Neurosci*. 2005;25(34):7709-7717. doi:10.1523/JNEUROSCI.2177-05.2005

31. Crossley NA, Mechelli A, Scott J, et al. The hubs of the human connectome are generally implicated in the anatomy of brain disorders. *Brain*. 2014;137(8):2382-2395. doi:10.1093/brain/awu132

32. Buckner RL. Memory and Executive Function in Aging and AD. *Neuron*. 2004;44(1):195-208. doi:10.1016/j.neuron.2004.09.006

33. Shafiei G, Markello RD, Makowski C, et al. Spatial Patterning of Tissue Volume Loss in Schizophrenia Reflects Brain Network Architecture. *Biological Psychiatry*. 2020;87(8):727-735. doi:10.1016/j.biopsych.2019.09.031

34. Shafiei G, Bazinet V, Dadar M, et al. Network structure and transcriptomic vulnerability shape atrophy in frontotemporal dementia. *Brain*. Published online February 21, 2022:awac069. doi:10.1093/brain/awac069

35. Krishnan A, Williams LJ, McIntosh AR, Abdi H. Partial Least Squares (PLS) methods for neuroimaging: A tutorial and review. *NeuroImage*. 2011;56(2):455-475. doi:10.1016/j.neuroimage.2010.07.034

36. Petersen M, Nägele FL, Mayer C, et al. Brain network architecture constrains age-related cortical thinning. *NeuroImage*. 2022;264:119721. doi:10.1016/j.neuroimage.2022.119721

37. Libby P, Ridker PM, Maseri A. Inflammation and atherosclerosis. *Circulation*. 2002;105(9):1135-1143. doi:10.1161/hc0902.104353

38. Birdsill AC, Carlsson CM, Willette AA, et al. Low cerebral blood flow is associated with lower memory function in metabolic syndrome. *Obesity*. 2013;21(7):1313-1320. doi:10.1002/oby.20170

39. Rimmele DL, Petersen EL, Schlemm E, et al. Association of Carotid Plaque and Flow Velocity With White Matter Integrity in a Middle-aged to Elderly Population. *Neurology*. Published online September 19, 2022. doi:10.1212/WNL.0000000000201297

40. Hadi HA, Carr CS, Al Suwaidi J. Endothelial Dysfunction: Cardiovascular Risk Factors, Therapy, and Outcome. *Vasc Health Risk Manag*. 2005;1(3):183-198.

41. Lind L. Endothelium-dependent vasodilation, insulin resistance and the metabolic syndrome in an elderly cohort: The Prospective Investigation of the Vasculature in Uppsala Seniors (PIVUS) study.

Atherosclerosis. 2008;196(2):795-802. doi:10.1016/j.atherosclerosis.2007.01.014

42. Hussain B, Fang C, Chang J. Blood–Brain Barrier Breakdown: An Emerging Biomarker of Cognitive Impairment in Normal Aging and Dementia. *Frontiers in Neuroscience*. 2021;15. Accessed November 9, 2022. https://www.frontiersin.org/articles/10.3389/fnins.2021.688090

43. Mullins CA, Gannaban RB, Khan MS, et al. Neural Underpinnings of Obesity: The Role of Oxidative Stress and Inflammation in the Brain. *Antioxidants (Basel)*. 2020;9(10):1018. doi:10.3390/antiox9101018

44. Wardlaw JM, Smith EE, Biessels GJ, et al. Neuroimaging standards for research into small vessel disease and its contribution to ageing and neurodegeneration. *The Lancet Neurology*. 2013;12(8):822-838. doi:10.1016/S1474-4422(13)70124-8

45. Frey BM, Petersen M, Mayer C, Schulz M, Cheng B, Thomalla G. Characterization of White Matter Hyperintensities in Large-Scale MRI-Studies. *Front Neurol*. 2019;10. doi:10.3389/fneur.2019.00238

46. Kotkowski E, Price LR, Franklin C, et al. A neural signature of metabolic syndrome. *Hum Brain Mapp*. Published online May 7, 2019:hbm.24617. doi:10.1002/hbm.24617

47. Leritz EC, Salat DH, Williams VJ, et al. Thickness of the human cerebral cortex is associated with metrics of cerebrovascular health in a normative sample of community dwelling older adults. *NeuroImage*. 2011;54(4):2659-2671. doi:10.1016/j.neuroimage.2010.10.050

48. Tuulari JJ, Karlsson HK, Hirvonen J, Salminen P, Nuutila P, Nummenmaa L. Neural Circuits for Cognitive Appetite Control in Healthy and Obese Individuals: An fMRI Study. *PLOS ONE*. 2015;10(2):e0116640. doi:10.1371/journal.pone.0116640

49. Rolls ET. The orbitofrontal cortex and reward. *Cereb Cortex*. 2000;10(3):284-294. doi:10.1093/cercor/10.3.284

50. Rolls ET. Reward Systems in the Brain and Nutrition. *Annu Rev Nutr*. 2016;36(1):435-470. doi:10.1146/annurev-nutr-071715-050725

51. Golchert J, Smallwood J, Jefferies E, et al. In need of constraint: Understanding the role of the cingulate cortex in the impulsive mind. *Neuroimage*. 2017;146:804-813. doi:10.1016/j.neuroimage.2016.10.041

52. Torregrossa MM, Quinn JJ, Taylor JR. Impulsivity, Compulsivity, and Habit: The Role of Orbitofrontal Cortex Revisited. *Biol Psychiatry*. 2008;63(3):253-255. doi:10.1016/j.biopsych.2007.11.014

53. Rolls ET. The orbitofrontal cortex, food reward, body weight and obesity. *Social Cognitive and Affective Neuroscience*. Published online April 8, 2021:nsab044. doi:10.1093/scan/nsab044

54. Price AE, Stutz SJ, Hommel JD, Anastasio NC, Cunningham KA. Anterior insula activity regulates the associated behaviors of high fat food binge intake and cue reactivity in male rats. *Appetite*. 2019;133:231-239. doi:10.1016/j.appet.2018.11.011

55. Krishnadas R, McLean J, Batty DG, et al. Cardio-metabolic risk factors and cortical thickness in a neurologically healthy male population: Results from the psychological, social and biological determinants of ill health (pSoBid) study. *NeuroImage: Clinical*. 2013;2:646-657. doi:10.1016/j.nicl.2013.04.012

56. Qin Q, Yin Y, Xing Y, et al. Lipid Metabolism in the Development and Progression of Vascular Cognitive Impairment: A Systematic Review. *Frontiers in Neurology*. 2021;12. Accessed November 4, 2022. https://www.frontiersin.org/articles/10.3389/fneur.2021.709134

57. Varma VR, Büşra Lüleci H, Oommen AM, et al. Abnormal brain cholesterol homeostasis in Alzheimer's disease—a targeted metabolomic and transcriptomic study. *npj Aging Mech Dis*. 2021;7(1):1-14. doi:10.1038/s41514-021-00064-9

58. Genon S, Eickhoff SB, Kharabian S. Linking interindividual variability in brain structure to behaviour. *Nat Rev Neurosci*. Published online April 1, 2022:1-12. doi:10.1038/s41583-022-00584-7

59. Bokura H, Nagai A, Oguro H, Kobayashi S, Yamaguchi S. The association of metabolic syndrome with executive dysfunction independent of subclinical ischemic brain lesions in Japanese adults. *Dement Geriatr Cogn Disord*. 2010;30(6):479-485. doi:10.1159/000322057

60. Hassenstab JJ, Sweat V, Bruehl H, Convit A. Metabolic syndrome is associated with learning and recall impairment in middle age. *Dement Geriatr Cogn Disord*. 2010;29(4):356-362. doi:10.1159/000296071

61. Gierach M, Rasmus A, Orłowska E. Verbal Fluency in Metabolic Syndrome. *Brain Sci*. 2022;12(2):255. doi:10.3390/brainsci12020255

62. Laurent JS, Watts R, Adise S, et al. Associations Among Body Mass Index, Cortical Thickness, and Executive Function in Children. *JAMA Pediatrics*. 2020;174(2):170-177. doi:10.1001/jamapediatrics.2019.4708

63. Seo SW, Ahn J, Yoon U, et al. Cortical Thinning in Vascular Mild Cognitive Impairment and Vascular Dementia of Subcortical Type. *Journal of Neuroimaging*. 2010;20(1):37-45. doi:10.1111/j.1552-6569.2008.00293.x

64. Kim HJ, Ye BS, Yoon CW, et al. Cortical thickness and hippocampal shape in pure vascular mild cognitive impairment and dementia of subcortical type. *Eur J Neurol*. 2014;21(5):744-751. doi:10.1111/ene.12376

65. Sashindranath M, Nandurkar HH. Endothelial Dysfunction in the Brain: Setting the Stage for Stroke and Other Cerebrovascular Complications of COVID-19. *Stroke*. 2021;52(5):1895-1904. doi:10.1161/STROKEAHA.120.032711

66. Denes A, Drake C, Stordy J, et al. Interleukin-1 Mediates Neuroinflammatory Changes Associated With Diet-Induced Atherosclerosis. *Journal of the American Heart Association*. 1(3):e002006. doi:10.1161/JAHA.112.002006

67. Tucsek Z, Toth P, Sosnowska D, et al. Obesity in Aging Exacerbates Blood–Brain Barrier Disruption, Neuroinflammation, and Oxidative Stress in the Mouse Hippocampus: Effects on Expression of Genes Involved in Beta-Amyloid Generation and Alzheimer's Disease. *The Journals of Gerontology: Series A*. 2014;69(10):1212-1226. doi:10.1093/gerona/glt177

68. Dheen ST, Kaur C, Ling EA. Microglial activation and its implications in the brain diseases. *Curr Med Chem*. 2007;14(11):1189-1197. doi:10.2174/092986707780597961

69. Lake BB, Ai R, Kaeser GE, et al. Neuronal subtypes and diversity revealed by single-nucleus RNA sequencing of the human brain. *Science*. 2016;352(6293):1586-1590. doi:10.1126/science.aaf1204

70. Pantoni L. Cerebral small vessel disease: from pathogenesis and clinical characteristics to therapeutic challenges. *The Lancet Neurology*. 2010;9(7):689-701. doi:10.1016/S1474-4422(10)70104-6

71. Petersen M, Frey BM, Mayer C, et al. Fixel based analysis of white matter alterations in early stage cerebral small vessel disease. *Sci Rep*. 2022;12(1):1581. doi:10.1038/s41598-022-05665-2

72. Petersen M, Frey BM, Schlemm E, et al. Network Localisation of White Matter Damage in Cerebral Small Vessel Disease. *Scientific Reports*. 2020;10(1):9210. doi:10.1038/s41598-020-66013-w

73. Alfaro FJ, Gavrieli A, Saade-Lemus P, Lioutas VA, Upadhyay J, Novak V. White matter microstructure and cognitive decline in metabolic syndrome: A review of diffusion tensor imaging. *Metabolism*. 2018;78:52-68. doi:10.1016/j.metabol.2017.08.009

74. Mayer C, Frey BM, Schlemm E, et al. Linking cortical atrophy to white matter hyperintensities of presumed vascular origin: *Journal of Cerebral Blood Flow & Metabolism*. Published online December 1, 2020. doi:10.1177/0271678X20974170

75. Segura B, Jurado MA, Freixenet N, Falcón C, Junqué C, Arboix A. Microstructural white matter changes in metabolic syndrome: a diffusion tensor imaging study. *Neurology*. 2009;73(6):438-444. doi:10.1212/WNL.0b013e3181b163cd

76. Saxena S, Caroni P. Selective Neuronal Vulnerability in Neurodegenerative Diseases: from Stressor Thresholds to Degeneration. *Neuron*. 2011;71(1):35-48. doi:10.1016/j.neuron.2011.06.031

77. Miller KL, Alfaro-Almagro F, Bangerter NK, et al. Multimodal population brain imaging in the UK Biobank prospective epidemiological study. *Nat Neurosci*. 2016;19(11):1523-1536. doi:10.1038/nn.4393

78. Jagodzinski A, Koch-gromus U, Adam G, Anders S, Augustin M. Rationale and Design of the Hamburg City Health Study. *European Journal of Epidemiology*. Published online 2019. doi:10.1007/s10654-019-00577-4

79. Veldsman M, Tai XY, Nichols T, et al. Cerebrovascular risk factors impact frontoparietal network integrity and executive function in healthy ageing. *Nat Commun*. 2020;11(1):4340. doi:10.1038/s41467-020-18201-5

80. Sudlow C, Gallacher J, Allen N, et al. UK Biobank: An Open Access Resource for Identifying the Causes of a Wide Range of Complex Diseases of Middle and Old Age. *PLoS Med*. 2015;12(3):e1001779. doi:10.1371/journal.pmed.1001779

81. Fawns-Ritchie C, Deary IJ. Reliability and validity of the UK Biobank cognitive tests. *PLoS One*. 2020;15(4):e0231627. doi:10.1371/journal.pone.0231627

82. Campagna F, Montagnese S, Ridola L, et al. The animal naming test: An easy tool for the assessment of hepatic encephalopathy. *Hepatology*. 2017;66(1):198-208. doi:10.1002/hep.29146

83. Folstein MF, Folstein SE, McHugh PR. "Mini-mental state". A practical method for grading the cognitive state of patients for the clinician. *J Psychiatr Res*. 1975;12(3):189-198. doi:10.1016/0022-3956(75)90026-6

84. Tombaugh T. Trail Making Test A and B: Normative data stratified by age and education. *Archives of Clinical Neuropsychology*. 2004;19(2):203-214. doi:10.1016/S0887-6177(03)00039-8

85. Moms JC, Heyman A, Mohs RC, et al. The Consortium to Establish a Registry for Alzheimer's Disease (CERAD). Part I. Clinical and neuropsychological assesment of Alzheimer's disease. *Neurology*. 1989;39(9):1159-1159. doi:10.1212/WNL.39.9.1159

86. Shulman KI. Clock-drawing: is it the ideal cognitive screening test? *International Journal of Geriatric Psychiatry*. 2000;15(6):548-561. doi:10.1002/1099-1166(200006)15:6<548::AID-GPS242>3.0.CO;2-U

87. Dahnke R, Yotter RA, Gaser C. Cortical thickness and central surface estimation. *NeuroImage*. 2013;65:336-348. doi:10.1016/j.neuroimage.2012.09.050

88. Gaser C, Dahnke R, Thompson PM, Kurth F, Luders E, Initiative ADN. CAT – A Computational Anatomy Toolbox for the Analysis of Structural MRI Data. Published online June 13, 2022:2022.06.11.495736. doi:10.1101/2022.06.11.495736

89. Yotter RA, Dahnke R, Thompson PM, Gaser C. Topological correction of brain surface meshes using spherical harmonics. *Hum Brain Mapp*. 2011;32(7):1109-1124. doi:10.1002/hbm.21095

90. Yotter RA, Thompson PM, Gaser C. Algorithms to Improve the Reparameterization of Spherical Mappings of Brain Surface Meshes. *Journal of Neuroimaging*. 2011;21(2):e134-e147. doi:10.1111/j.1552-6569.2010.00484.x

91. Wagner AS, Waite LK, Wierzba M, et al. FAIRly big: A framework for computationally reproducible processing of large-scale data. *Sci Data*. 2022;9(1):80. doi:10.1038/s41597-022-01163-2

92. Halchenko Y, Meyer K, Poldrack B, et al. DataLad: distributed system for joint management of code, data, and their relationship. *JOSS*. 2021;6(63):3262. doi:10.21105/joss.03262

93. Rubinov M, Sporns O. Complex network measures of brain connectivity: uses and interpretations. *Neuroimage*. 2010;52(3):1059-1069. doi:10.1016/j.neuroimage.2009.10.003

94. Larivière S, Bayrak Ş, Vos de Wael R, et al. BrainStat: A toolbox for brain-wide statistics and multimodal feature associations. *Neuroimage*. 2023;266:119807. doi:10.1016/j.neuroimage.2022.119807

95. Burt JB, Helmer M, Shinn M, Anticevic A, Murray JD. Generative modeling of brain maps with spatial autocorrelation. *NeuroImage*. 2020;220:117038. doi:10.1016/j.neuroimage.2020.117038

96. Larivière S, Paquola C, Park B yong, et al. The ENIGMA Toolbox: multiscale neural contextualization of multisite neuroimaging datasets. *Nat Methods*. 2021;18(7):698-700. doi:10.1038/s41592-021-01186-4

97. Markello RD, Hansen JY, Liu ZQ, et al. neuromaps: structural and functional interpretation of brain maps. *Nat Methods*. Published online October 6, 2022:1-8. doi:10.1038/s41592-022-01625-w

98. Caswell TA, Droettboom M, Lee A, et al. matplotlib/matplotlib: REL: v3.5.2. Published online May 3, 2022. doi:10.5281/zenodo.6513224

99. Harris CR, Millman KJ, van der Walt SJ, et al. Array programming with NumPy. *Nature*. 2020;585(7825):357-362. doi:10.1038/s41586-020-2649-2

100. Reback J, McKinney W, jbrockmendel, et al. pandas-dev/pandas: Pandas 1.0.3. Published online March 18, 2020. doi:10.5281/zenodo.3715232

101. Vallat R. Pingouin: statistics in Python. *JOSS*. 2018;3(31):1026. doi:10.21105/joss.01026

102. Abraham A, Pedregosa F, Eickenberg M, et al. Machine learning for neuroimaging with scikit-learn. *Frontiers in Neuroinformatics*. 2014;8. Accessed March 28, 2022. https://www.frontiersin.org/article/10.3389/fninf.2014.00014

103. Waskom ML. seaborn: statistical data visualization. *Journal of Open Source Software*. 2021;6(60):3021. doi:10.21105/joss.03021

104. Lotter L. LeonDLotter/ABAnnotate: 0.1.1. Published online June 14, 2022. doi:10.5281/zenodo.6640855

105. Rahim M, Thirion B, Varoquaux G. Multi-output predictions from neuroimaging: assessing reduced-rank linear models. In: *2017 International Workshop on Pattern Recognition in Neuroimaging (PRNI)*. ; 2017:1-4. doi:10.1109/PRNI.2017.7981504

106. Schaefer A, Kong R, Gordon EM, et al. Local-Global Parcellation of the Human Cerebral Cortex from Intrinsic Functional Connectivity MRI. *Cerebral Cortex*. 2018;28(9):3095-3114. doi:10.1093/cercor/bhx179

107. Darmanis S, Sloan SA, Zhang Y, et al. A survey of human brain transcriptome diversity at the single cell level. *Proceedings of the National Academy of Sciences*. 2015;112(23):7285-7290. doi:10.1073/pnas.1507125112

108. Wang D, Liu S, Warrell J, et al. Comprehensive functional genomic resource and integrative model for the human brain. *Science*. 2018;362(6420):eaat8464. doi:10.1126/science.aat8464

109. Markello RD, Arnatkeviciute A, Poline JB, Fulcher BD, Fornito A, Misic B. Standardizing workflows in imaging transcriptomics with the abagen toolbox. Jbabdi S, Makin TR, Jbabdi S, Burt J, Hawrylycz MJ, eds. *eLife*. 2021;10:e72129. doi:10.7554/eLife.72129

110. Arnatkeviciute A, Fulcher BD, Fornito A. A practical guide to linking brain-wide gene expression and neuroimaging data. *Neuroimage*. 2019;189:353-367. doi:10.1016/j.neuroimage.2019.01.011

111. Hawrylycz MJ, Lein ES, Guillozet-Bongaarts AL, et al. An anatomically comprehensive atlas of the adult human brain transcriptome. *Nature*. 2012;489(7416):391-399. doi:10.1038/nature11405

112. Dukart J, Holiga S, Rullmann M, et al. JuSpace: A tool for spatial correlation analyses of magnetic resonance imaging data with nuclear imaging derived neurotransmitter maps. *Hum Brain Mapp*. 2021;42(3):555-566. doi:10.1002/hbm.25244

113. Fulcher BD, Arnatkeviciute A, Fornito A. Overcoming false-positive gene-category enrichment in the analysis of spatially resolved transcriptomic brain atlas data. *Nat Commun*. 2021;12(1):2669. doi:10.1038/s41467-021-22862-1

114. Burt JB, Demirtaş M, Eckner WJ, et al. Hierarchy of transcriptomic specialization across human cortex captured by structural neuroimaging topography. *Nat Neurosci*. 2018;21(9):1251-1259. doi:10.1038/s41593-018-0195-0

115. Larivière S, Rodríguez-Cruces R, Royer J, et al. Network-based atrophy modeling in the common epilepsies: A worldwide ENIGMA study. *Sci Adv*. 2020;6(47):eabc6457. doi:10.1126/sciadv.abc6457

116. van den Heuvel MP, Sporns O. Network hubs in the human brain. *Trends in Cognitive Sciences*. 2013;17(12):683-696. doi:10.1016/j.tics.2013.09.012

117. Margulies DS, Ghosh SS, Goulas A, et al. Situating the default-mode network along a principal gradient of macroscale cortical organization. *Proc Natl Acad Sci U S A*. 2016;113(44):12574-12579. doi:10.1073/pnas.1608282113

118. Sydnor VJ, Larsen B, Bassett DS, et al. Neurodevelopment of the association cortices: Patterns, mechanisms, and implications for psychopathology. *Neuron*. 2021;109(18):2820-2846. doi:10.1016/j.neuron.2021.06.016

119. Vos de Wael R, Benkarim O, Paquola C, et al. BrainSpace: a toolbox for the analysis of macroscale gradients in neuroimaging and connectomics datasets. *Communications Biology*. 2020;3(1):1-10. doi:10.1038/s42003-020-0794-7

120. Alexander-Bloch AF, Shou H, Liu S, et al. On testing for spatial correspondence between maps of human brain structure and function. *NeuroImage*. 2018;178:540-551. doi:10.1016/j.neuroimage.2018.05.070

121. Maslov S, Sneppen K, Zaliznyak A. Pattern Detection in Complex Networks: Correlation Profile of the Internet. *Physica A: Statistical Mechanics and its Applications*. 2004;333:529-540. doi:10.1016/j.physa.2003.06.002

Acknowledgements

The authors wish to acknowledge all participants of the UK Biobank and Hamburg City Health Study. Special thanks applies to the staff at the Epidemiological Study Center for conducting the HCHS. The participating institutes and departments from the University Medical Center Hamburg-Eppendorf contribute all with individual and scaled budgets to the overall funding. The publication has been approved by the Steering Board of the Hamburg City Health Study.

Funding

This work was supported by grants from the German Research Foundation (Deutsche Forschungsgemeinschaft, DFG): Schwerpunktprogramm (SPP) 204, project number 454012190 as well as Sonderforschungsbereich (SFB) 936, project number 178316478, Project C2 (M.P., C.M., J.F., G.T., and B.C.) & C7 (S.K., J.G.). Furthermore, SBE acknowledges funding by the European Union's Horizon 2020 Research and Innovation Program (grant agreements 945539 (HBP SGA3) and 826421 (VBC)), the Deutsche Forschungsgemeinschaft (DFG, SFB 1451 & IRTG 2150) and the National Institute of Health (R01 MH074457). The Hamburg City Health Study is also supported by Amgen, Astra Zeneca, Bayer, BASF, Deutsche Gesetzliche Unfallversicherung (DGUV), Deutsches Institut für Ernährungsforschung, the Innovative medicine initiative (IMI) under grant number No. 116074, the Fondation Leducq under grant number 16 CVD 03., the euCanSHare grant agreement under grant number 825903-euCanSHare H2020, Novartis, Pfizer, Schiller, Siemens, Unilever and "Förderverein zur Förderung der HCHS e.V.".

Author contributions

Each author has made a significant contribution to the manuscript and all authors read and approved its final version. We describe individual contributions to the paper using the CRediT contributor role taxonomy. Conceptualization: M.P., F.H., B.C.; Data Curation: M.P., F.H., F.N., C.M., M.S.; Formal analysis: M.P.; Funding acquisition: S.B.E., G.T., B.C.; Investigation: M.P.; Methodology: M.P.; Software: M.P., F.H.; Supervision: G.T., B.C.; Visualization: M.P.; Writing—original draft: M.P.; Writing—review & editing: M.P., F.H., F.N., C.M., M.S., L.R., B.Z., T.Z., S.K., J.G., J.F., R.T., A.O., K.P., S.B.E., G.T., B.C.

Competing interest statement

JG has received speaker fees from Lundbeck, Janssen-Cilag, Lilly, Otsuka and Boehringer outside the submitted work. JF reported receiving personal fees from Acandis, Cerenovus, Microvention, Medtronic, Phenox, and Penumbra; receiving grants from Stryker and Route 92; being managing director of eppdata; and owning shares in Tegus and Vastrax; all outside the submitted work. GT has received fees as consultant or lecturer from Acandis, Alexion, Amarin, Bayer, Boehringer Ingelheim, BristolMyersSquibb/Pfizer, Daichi Sankyo, Portola, and Stryker outside the submitted work. The remaining authors declare no conflicts of interest.

Data availability

UK Biobank data can be obtained via its standardized data access procedure (https://www.ukbiobank.ac.uk/). HCHS participant data used in this analysis is not publicly available for privacy reasons.

Code availability

The analysis code is publicly available on GitHub (https://github.com/csi-hamburg/2023_petersen_mets_cortical_thickness and https://github.com/csi-hamburg/CSIframe/wiki/Structural-processing-with-CAT).

Table 1. Descriptive statistics UKB and HCHS

Metric	*Stat*[a]
Age (years)	63.55 ± 7.59 (40087)
Sex (% female)	46.47 (40087)
Education (ISCED)	2.62 ± 0.73 (39944)
Metabolic syndrome components	
Waist circumference (cm)	88.47 ± 12.71 (38800)
Hip circumference (cm)	100.90 ± 8.79 (38801)
Waist-hip ratio	0.88 ± 0.09 (38800)
Body mass index	26.47 ± 4.37 (38701)
$RR_{systolic}$ (mmHg)	138.30 ± 18.57 (31234)
$RR_{diastolic}$ (mmHg)	78.88 ± 10.09 (31238)
Antihypertensive therapy (%)	6.96 (39976)
HDL (mg/dL)	61.76 ± 23.69 (34468)
LDL (mg/dL)	137.38 ± 36.29 (37456)
Cholesterol (mg/dL)	211.29 ± 56.42 (37531)
Triglycerides (mg/dL)	148.90 ± 83.84 (37510)
Lipid lowering therapy (%)	14.44 (39976)
Blood glucose (mg/dL)	90.29 ± 17.58 (34432)
Antidiabetic therapy (%)	0.45 (39976)
Imaging	
Mean cortical thickness (mm)	2.40 ± 0.09 (40087)
Cognitive variables of the UK Biobank	
Fluid Intelligence	6.63 ± 2.06 (36510)
Matrix Pattern Completion	7.99 ± 2.13 (25771)
Numeric Memory Test	6.69 ± 1.52 (26780)
Paired Associate Learning	6.92 ± 2.63 (26048)
Prospective Memory	1.07 ± 0.39 (37192)
Reaction Time (sec)	594.16 ± 109.08 (37015)

Symbol Digit Substitution	18.96 ± 5.25 (25810)
Tower Rearranging Test	9.91 ± 3.23 (25555)
Trail Making Test A (sec)	223.03 ± 86.51 (26048)
Trail Making Test B (sec)	550.01 ± 270.09 (26048)
Cognitive variables of the Hamburg City Health Study	
Animal Naming Test	24.78 ± 6.92 (2416)
Clock Drawing Test	6.43 ± 1.12 (2479)
Trail Making Test A (sec)	40.09 ± 14.33 (2290)
Trail Making Test B (sec)	90.05 ± 37.30 (2264)
Multiple-Choice Vocabulary Intelligence Test	31.27 ± 3.58 (2026)
Word List Recall	7.75 ± 1.84 (2342)

Abbreviations: cm = centimeter, dL = deciliter, HDL = high density lipoprotein, ISCED = International Standard Classification of Education, mg = milligram, mm = millimeters, mmHg = millimeters of mercury, RR = Blood pressure, sec = seconds
[a]Presented as mean ± SD (N)

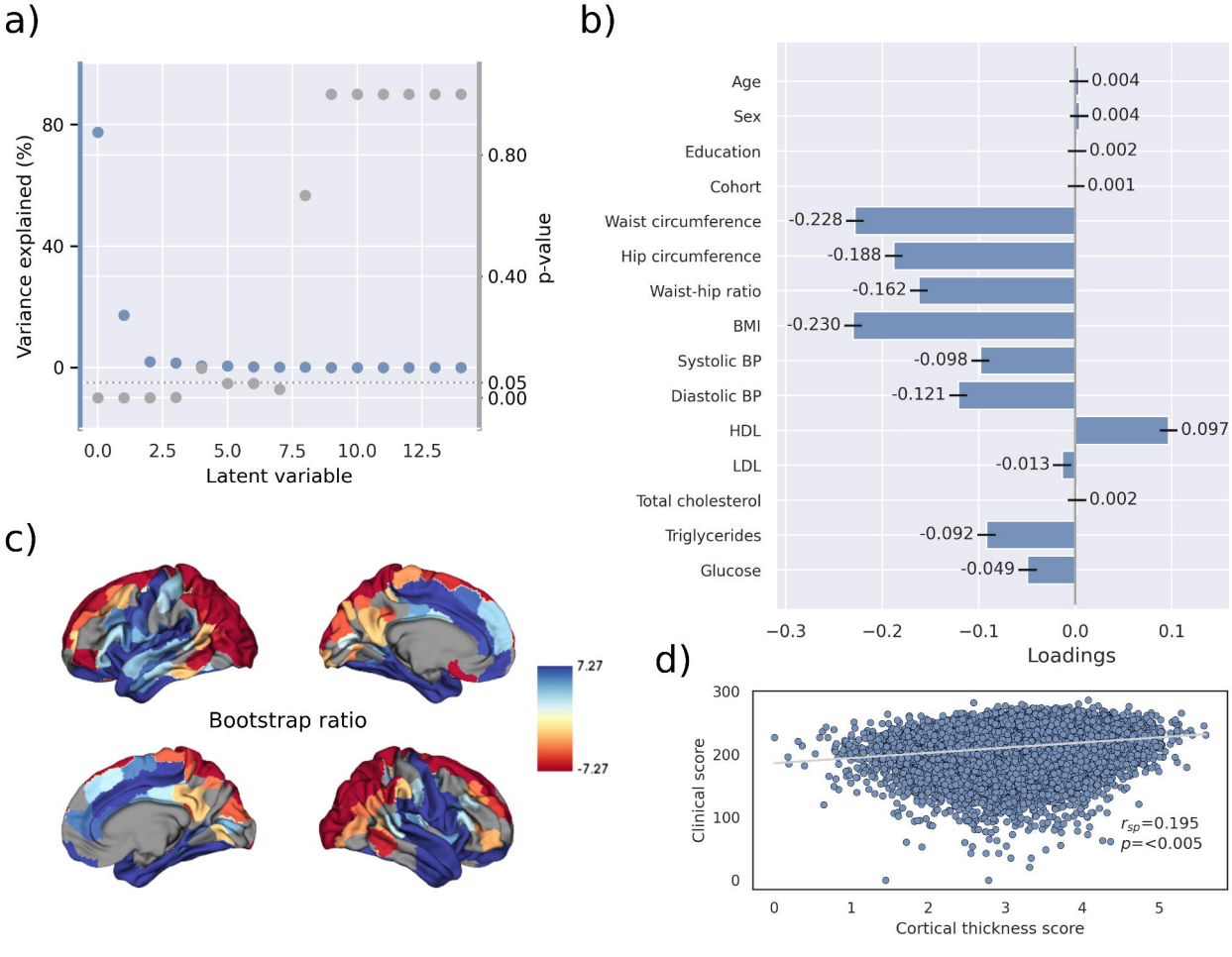
a)
Variance explained (%)
80
40
0
0.80
0.40
0.05
0.00
p-value
0.0
2.5
5.0
7.5
10.0
12.5
Latent variable
b)
Age
Sex
Education
Cohort
Waist circumference
Hip circumference
Waist-hip ratio
BMI
Systolic BP
Diastolic BP
HDL
LDL
Total cholesterol
Triglycerides
Glucose
0.004
0.004
0.002
0.001
-0.228
-0.188
-0.162
-0.230
-0.098
-0.121
0.097
-0.013
0.002
-0.092
-0.049
−0.3
−0.2
−0.1
0.0
0.1
Loadings
c)
Bootstrap ratio
7.27
-7.27
d)
Clinical score
300
200
100
0
r_{sp}=0.195
p=<0.005
0
1
2
3
4
5
Cortical thickness score

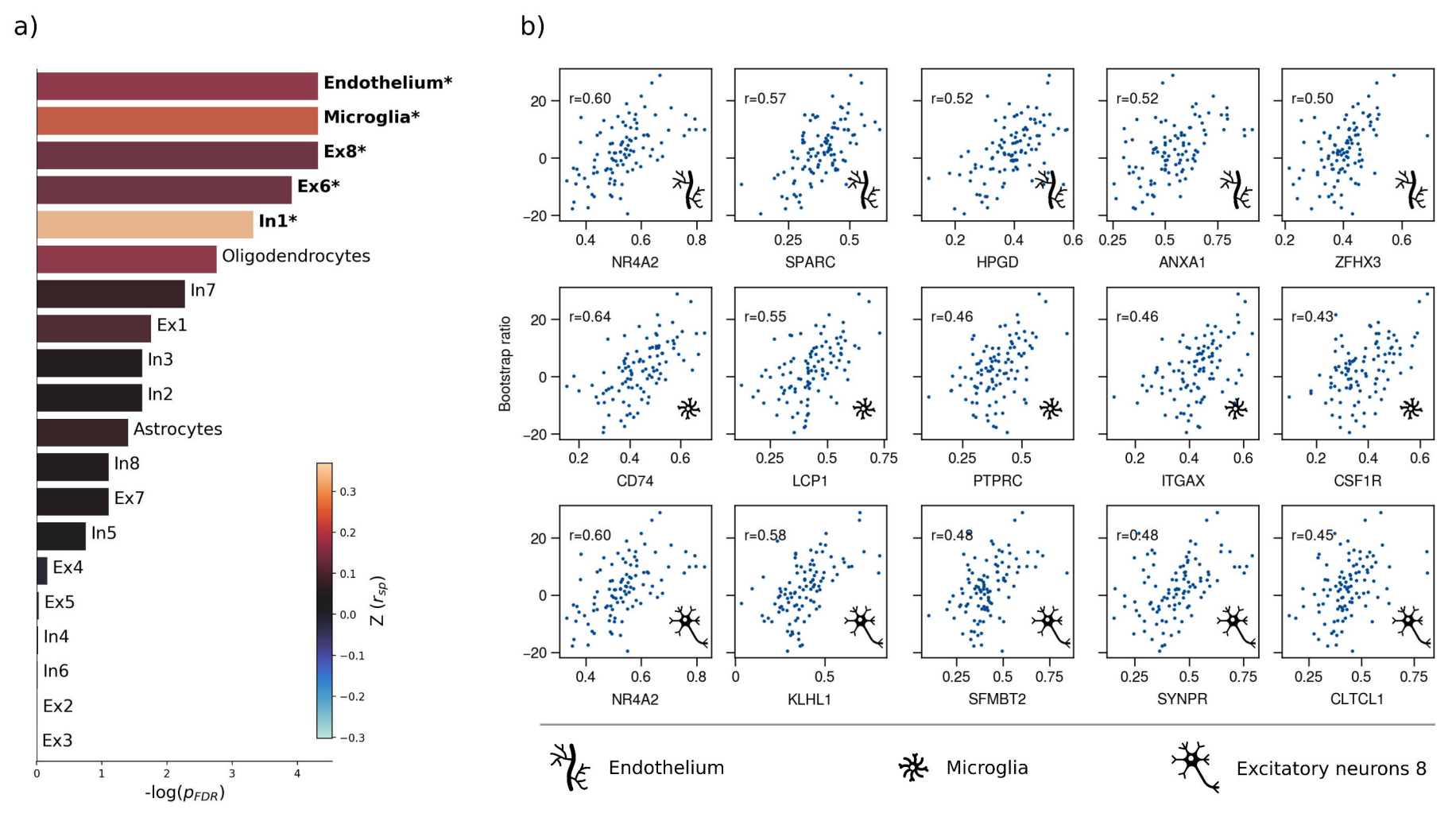
a)
Endothelium*
Microglia*
Ex8*
Ex6*
In1*
Oligodendrocytes
In7
Ex1
In3
In2
Astrocytes
In8
Ex7
In5
Ex4
Ex5
In4
In6
Ex2
Ex3
0
1
2
3
4
-log(p_{FDR})
0.3
0.2
0.1
0.0
−0.1
−0.2
−0.3
Z (r_{sp})
b)
Bootstrap ratio
r=0.60
NR4A2
r=0.57
SPARC
r=0.52
HPGD
r=0.52
ANXA1
r=0.50
ZFHX3
r=0.64
CD74
r=0.55
LCP1
r=0.46
PTPRC
r=0.46
ITGAX
r=0.43
CSF1R
r=0.60
NR4A2
r=0.58
KLHL1
r=0.48
SFMBT2
r=0.48
SYNPR
r=0.45
CLTCL1
Endothelium
Microglia
Excitatory neurons 8

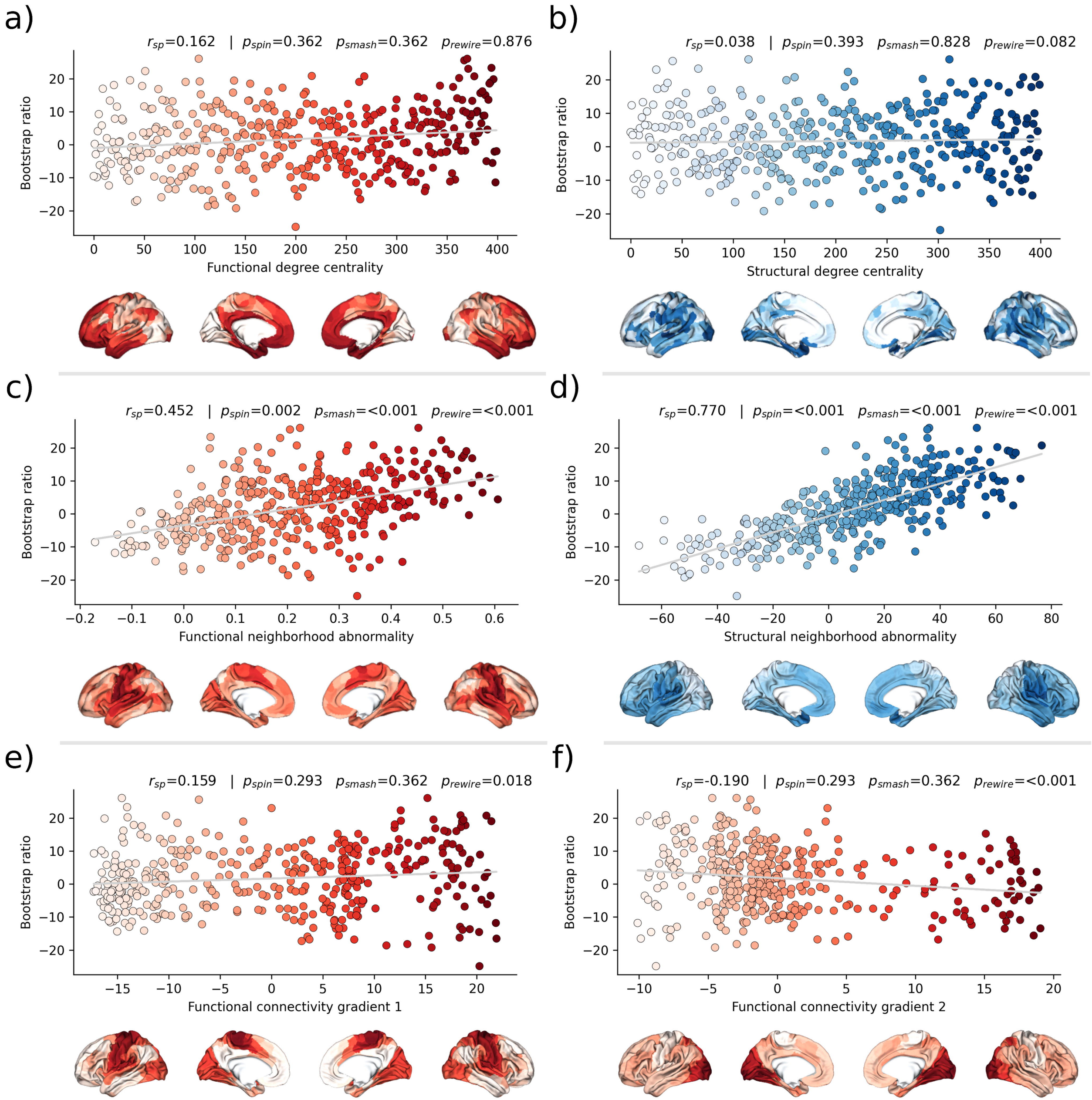
a)
r_{sp}=0.162 | p_{spin}=0.362 p_{smash}=0.362 p_{rewire}=0.876
Bootstrap ratio
Functional degree centrality
b)
r_{sp}=0.038 | p_{spin}=0.393 p_{smash}=0.828 p_{rewire}=0.082
Bootstrap ratio
Structural degree centrality
c)
r_{sp}=0.452 | p_{spin}=0.002 p_{smash}=<0.001 p_{rewire}=<0.001
Bootstrap ratio
Functional neighborhood abnormality
d)
r_{sp}=0.770 | p_{spin}=<0.001 p_{smash}=<0.001 p_{rewire}=<0.001
Bootstrap ratio
Structural neighborhood abnormality
e)
r_{sp}=0.159 | p_{spin}=0.293 p_{smash}=0.362 p_{rewire}=0.018
Bootstrap ratio
Functional connectivity gradient 1
f)
r_{sp}=-0.190 | p_{spin}=0.293 p_{smash}=0.362 p_{rewire}=<0.001
Bootstrap ratio
Functional connectivity gradient 2

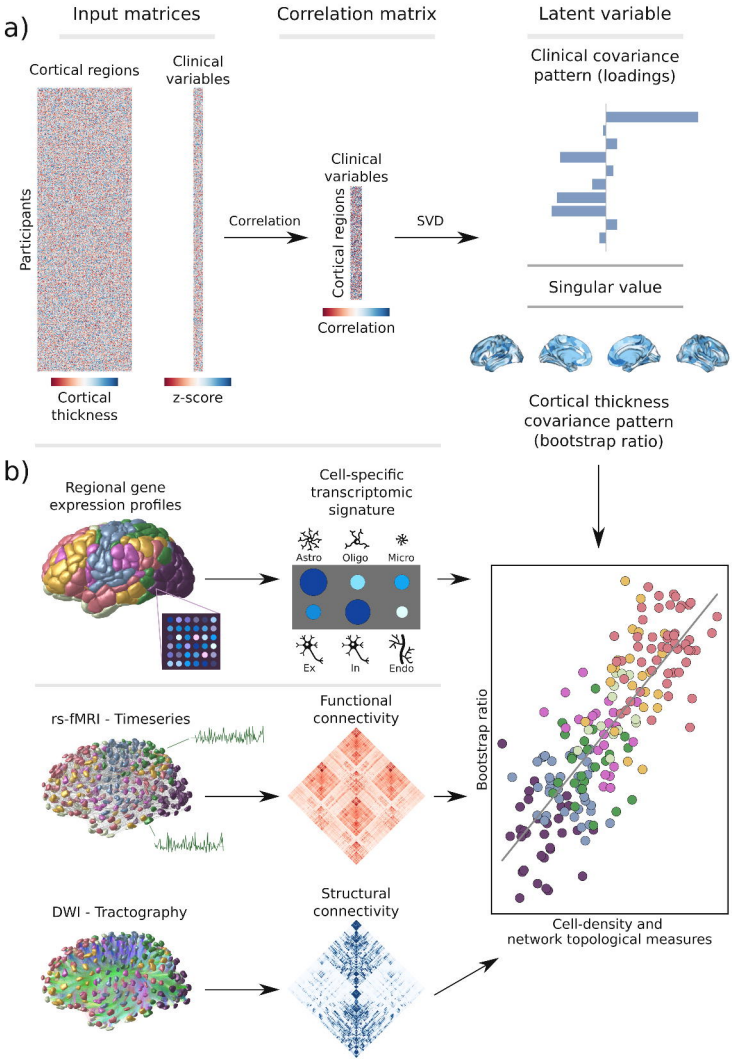
a)
Input matrices
Correlation matrix
Latent variable
Cortical regions
Clinical variables
Participants
Cortical thickness
z-score
Correlation
Clinical variables
Cortical regions
Correlation
SVD
Clinical covariance pattern (loadings)
Singular value
Cortical thickness covariance pattern (bootstrap ratio)
b)
Regional gene expression profiles
Cell-specific transcriptomic signature
Astro
Oligo
Micro
Ex
In
Endo
rs-fMRI - Timeseries
Functional connectivity
DWI - Tractography
Structural connectivity
Bootstrap ratio
Cell-density and network topological measures